

THE ROLE OF MORB AND SSZ MAGMA-TYPES IN THE FORMATION OF JURASSIC ULTRAMAFIC CUMULATES IN THE MIRDITA OPHIOLITES (ALBANIA) AS DEDUCED FROM CHROMIAN SPINEL AND OLIVINE CHEMISTRY

Emilio Saccani  and Renzo Tassinari

Dipartimento di Fisica e Scienze della Terra, Università di Ferrara, Italy.

 *Corresponding author, e-mail: sac@unife.it*

Keywords: *ophiolite, ultramafic cumulates, chromian spinel, olivine, Jurassic. Albania.*

ABSTRACT

Both the Western (WMO) and Eastern (EMO) Mirdita ophiolites include well-developed ultramafic cumulitic sequences. In the WMO, they mainly consist of dunites, plagioclase-dunites, plagioclase-wehrlites, and troctolites. In contrast, in the EMO they mainly consist of chromitiferous-dunites, dunites, lherzolites and olivine-websterites, as well as minor plagioclase-bearing dunites and lherzolites, and troctolites. The main rock-forming minerals in ultramafic cumulates are cumulus olivine associated with various inter-cumulus minerals, as well as chromian spinel occurring as both cumulus and inter-cumulus phase.

Mg#, FeO/MgO ratios and TiO₂, Al₂O₃ concentrations in parental melts were calculated from olivine and spinel compositions. The inferred parental melt compositions indicate that the dunite-troctolite layered series at the mantle tectonite-ultramafic cumulate transition zone in the WMO was derived from a normal-type mid-ocean ridge basaltic (N-MORB) parental melt. In contrast, the dunite-troctolite layered series from the top of the WMO ultramafic cumulitic sequence was derived from a medium-Ti basaltic (MTB) parental melt originated, in turn, in a nascent forearc setting.

The inferred composition of parental melts indicate that chromitiferous dunites, dunites, and lherzolites from the EMO were originated from primary boninitic melts, whereas olivine-websterites were originated from slightly fractionated boninitic liquids. The inferred parental melt compositions plagioclase-bearing dunites and lherzolites, as well as troctolites from the EMO are compatible with an N-MORB type parentage, being the only exception one plagioclase-dunite, which may have derived from a low-Ti tholeiitic melt. Comparison of the ultramafic cumulates from the WMO and EMO indicates that both these units, though to a different extent, have experienced similar and coeval magmatic events. The investigated WMO ultramafic cumulates record N-MORB and MTB magmatic episodes. The investigated EMO ultramafic cumulates testify for boninitic, N-MORB, and very subordinate low-Ti tholeiitic magmatic events. It is therefore concluded that both WMO and EMO were generated in a protoforearc-forearc setting likely initiated nearby an active mid-ocean spreading ridge.

INTRODUCTION

The Dinaride-Albanide-Hellenide orogenic belt is characterized by the occurrence of two NNW-SSE trending, parallel ophiolitic belts extending from the former Yugoslavian Republics to Greece, which are: 1) the internal (eastern) ophiolitic belt within the Axios-Vardar zone and 2) the external (western) ophiolitic belt extending from the Dinaride Ophiolite Belt to the Mirdita zone in Albania and the Sub-Pelagonian zone in Greece (e.g., Robertson and Shallo, 2000; Dilek et al., 2005; 2008; Saccani et al., 2011, and references therein). The earlier studies on the Mirdita ophiolites in central-north Albania led to the recognition of two ophiolitic units with distinct geology, petrology, geochemistry, and tectonic setting of formation, which were classically identified as the Western and Eastern Ophiolitic Belts (Shallo et al., 1990; Shallo, 1994; Beccaluva et al., 1994). According to this subdivision, the Western Mirdita ophiolites (WMO) were interpreted as a portion of Jurassic oceanic lithosphere generated at mid-oceanic ridge (MOR-type ophiolites), whereas the Eastern Mirdita ophiolites (EMO) were interpreted as a section of Jurassic oceanic lithosphere generated in a supra-subduction zone setting (SSZ-type ophiolites). However, the increasing number of researches carried out after earlier studies highlighted that this twofold subdivision was not so clear as previously thought. In fact, Bortolotti et al. (1996; 2002) described for the first time the occurrence of SSZ-type basalts interlayered within typical MOR basalts (MORB) in some volcanic sequences from the WMO. They also noticed that the uppermost part of these volcanic sequences is locally characterized by the occur-

rence of boninitic lava flows. Similar evidence was shown by Bébien et al. (2000) and Insergueix-Filippi et al. (2000). In the Pindos ophiolite, which can be considered as the continuation of the WMO in Greece, many authors showed, besides the MOR character, an SSZ contribution in the lavas and dykes (e.g., Capedri et al., 1982; Jones et al., 1991; Saccani and Photiades, 2004). Soon after, Manika et al. (1997) and Bébien et al. (1998) described the occurrence of typical MOR-type rocks in the Shebenik massif of the EMO unit (Fig.1). Later, Hoeck and Koller (1999), Hoeck et al. (2002), and Koller et al. (2006) showed that in southern Albania any distinction between WMO and EMO is far to be clear. They indeed described the occurrence of both lherzolitic (western-type) and harzburgitic (eastern-type) mantle tectonites in the same ophiolitic massif (e.g., Morava and Shpati), as well as minor SSZ fingerprint in the intrusive and volcanic sequences of the Voskopoja, Rehove and Morava massifs. Likewise, in Shpati and Luniku massifs, SSZ plutonic rocks occur together with a considerable amount of MOR-type gabbros (Koller et al., 2006).

From above, it is clear that both the WMO and EMO experienced a complex evolution of different magma types, which coexisted in both time and space. In turn, these distinct magma-types reflect generation from distinct mantle sources. In fact, four distinct types of basaltic rocks can be observed in the Jurassic volcanic sequences of the Mirdita ophiolites: 1) high-Ti mid-ocean ridge basalts showing normal compositions (N-MORB); 2) basalts with geochemical features intermediate between MORB and island arc tholeiites; hereafter defined, according to Saccani (2014), as medium-Ti basalts (MTB); 3) low-Ti, island arc tholeiitic

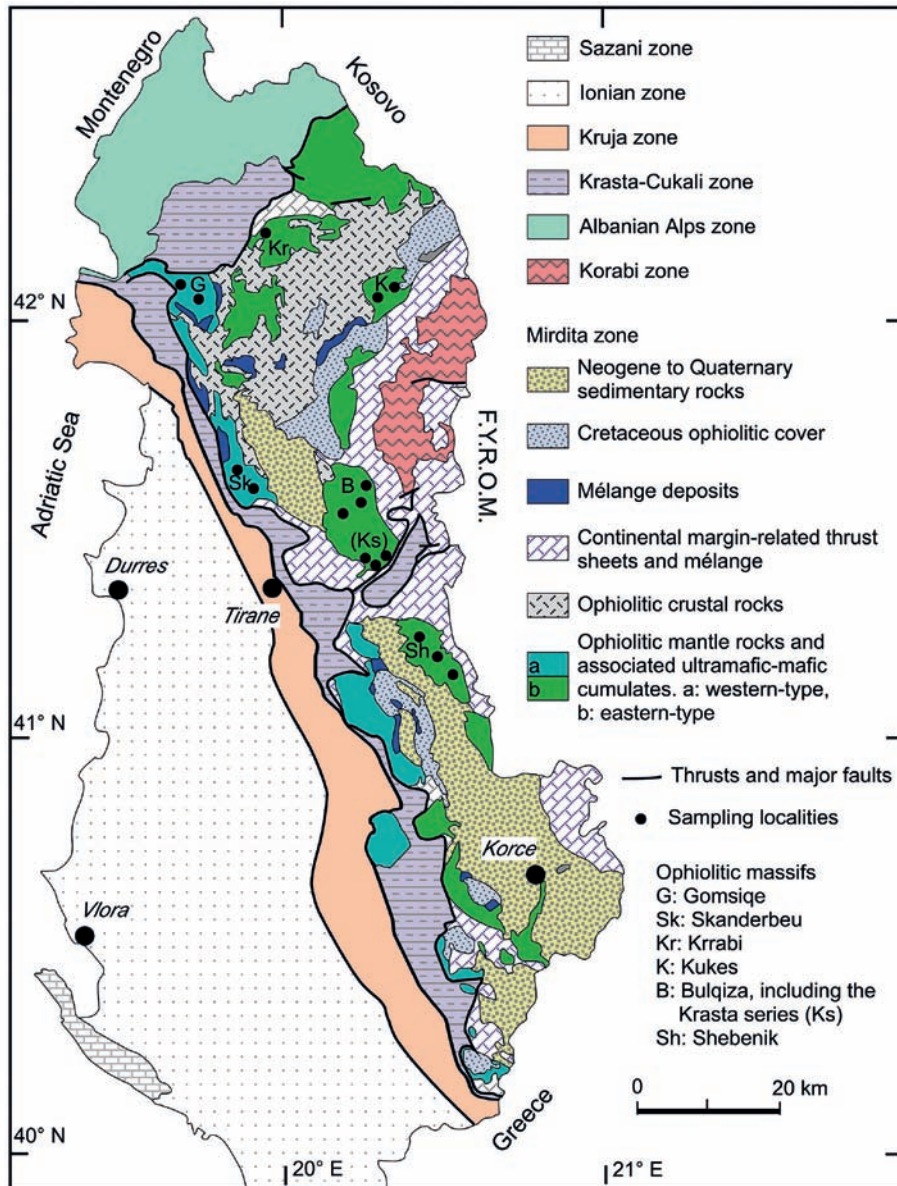


Fig. 1 - Simplified tectonic map of Albania (modified from Xhomo et al., 2002; Hoeck et al., 2014). Sampling localities are also shown.

(IAT) basalts; 4) very low-Ti boninitic basalts (e.g., Beccaluva et al., 1994; Bébien et al., 2000; Shallo, 1994; Bortolotti et al., 1996; 2002; Robertson and Shallo, 2000; Hoeck et al., 2002; Saccani et al., 2011). The complex interaction between different magma types is also observed in many cumulitic sequences of the Mirdita ophiolites. However, due to the cumulitic nature of these rocks, direct information about their parental magma composition is lacking because cumulitic rocks do not directly represent liquid compositions. Nonetheless, many authors have shown that the chemical compositions of chromian spinel and olivine are sensitive petrogenetic indicators and can be used to constrain the parental melt composition (e.g., Dick and Bullen, 1984; Augé, 1987; Ulmer, 1989; Arai, 1994; Kepezhinskas et al., 1993; Zhou et al., 1996; Kamenetsky et al., 2001; Rollinson, 2008). Therefore, new mineral chemistry data on chromian spinel and olivine from mantle tectonites and ultramafic-mafic cumulates from various localities of the Mirdita ophiolites (Fig. 1), are presented in this paper with the aim of constraining the geochemical characteristics of their associated parental melts.

GEOLOGICAL SETTING

The Albanide-Hellenide orogenic belt is composed of several westward-verging tectono-stratigraphic zones (Fig. 1), which can be referred to three fundamental paleo-tectonic settings (Bortolotti et al., 2013). They are (from west to east): 1) the Adria continental domain (represented by the Sazani, Ionian, Kruja, Krasta-Cukali and Albanian Alps zones); 2) the Mirdita ophiolitic domain; 3) the easternmost edge of the Adria continental domain (Korabi zone). Alternatively, some authors refer the Korabi zone to the western border of an independent microcontinental block known as the Korabi-Pelagonian microcontinent (e.g., Robertson, 1994; Robertson and Shallo, 2000; Dilek et al., 2005; 2008).

The Mirdita zone ophiolites (Fig. 1) represent remnants of Mesozoic oceanic lithosphere within the Dinaride-Hellenide segment of the Alpine orogenic system. They form a coherent, NNW-SSE trending belt and consist of a large variety of rocks attributed to originally complete oceanic lithospheric sequences. Many authors showed that although mainly composed of MORB-type rocks, the WMO also

include significant amounts of SSZ rocks, whereas minor volumes of typical MOR-type plutonic rocks are interlayered within the SSZ-type intrusive sequences of the EMO (e.g., Bortolotti et al., 1996; 2002; Manika et al., 1997; Bébien et al., 1998; 2000; Hoeck and Koller, 1999; Insergueix-Filippi et al., 2000; Hoeck et al., 2002; Koller et al., 2006; Saccani et al., 2011). Therefore, a generalized pseudo-stratigraphic scheme that resumes evidence from different localities of the Mirdita ophiolites is shown in Fig. 2.

Both WMO and EMO are associated throughout with the same sub-ophiolitic mélangé unit (Rubik Complex) with slices of metamorphic soles intercalated in-between. The mélangé unit consists of an assemblage of block and/or thrust sheets of (1) Triassic-Jurassic, mainly carbonate sequence; (2) serpentinized mantle peridotites; (3) Triassic basalts showing alkaline, enriched MORB, and N-MORB compositions; (4) Jurassic basalts showing N-MORB, MTB, and boninitic compositions (Bortolotti et al., 1996; Saccani and Photiadis, 2005).

The WMO pseudo-stratigraphic ophiolitic sequence (Fig. 2a) includes, from bottom to top: (1) mantle tectonites largely consisting of lherzolites and subordinate harzburgites; (2) a layered mafic-ultramafic cumulitic sequence; (3) a mafic to differentiated intrusive sequence; (4) a poorly developed sheeted dyke complex; and (5) a volcanic sequence. The layered mafic-ultramafic cumulitic sequence is largely composed of typical MORB-type rocks, including dunites, plagioclase-dunites, troctolites, wehrlites, mela-gabbros, and gabbros, where the observed crystallization order is: olivine \pm chromite followed by plagioclase and clinopyroxene (Beccaluva et al., 1983). Nonetheless, this sequence locally includes websterites and orthopyroxenites, especially in the southern Albania area (Hoeck et al., 2002; Koller et al., 2006). The upper intrusive sequence is largely dominated by gabbros with very scarce Fe-gabbros, plagiogranites and gabbronorites. The volcanic sequence includes volcanic series of pillow lava basalts with N-MORB affinity, as well as volcanic series where N-MORBs alternate with MTBs.

These series are cross cut by boninitic dykes and locally topped by boninitic lava flows (Bortolotti et al., 1996; 2002; Bébien et al., 2000; Hoeck et al., 2002; Saccani et al., 2011).

The reconstructed stratigraphic ophiolitic sequence of EMO (Fig. 2b) includes (from bottom to top): (1) mantle tectonites exclusively represented by variably depleted harzburgites; (2) a layered mafic-ultramafic cumulitic sequence; (3) a mafic to differentiated intrusive sequence; (4) a thick sheeted dyke complex; and (5) a volcanic sequence. Mantle harzburgites frequently show dunite and chromitite pods and lenses in their upper part. The abundance of these pods and lenses increase toward the top of the mantle section showing a transition to the overlying cumulates. Ultramafic cumulates consist of dunites with chromitite layers, olivine-websterites, and websterites. In these rocks, the typical crystallization order for SSZ-type rocks is observed (i.e., olivine \pm chromite, pyroxenes + plagioclase + magnetite, ilmenite). Locally, layers of plagioclase-lherzolites and troctolites occur in the cumulitic sequences of the Bulqiza and Shebenik ultramafic massifs (Beccaluva et al., 1994; Bébien et al., 1998), as well as in south Albania (Koller et al., 2006). Both cumulitic and isotropic mafic rocks are largely dominated by olivine-gabbronorites and gabbronorites and are followed by abundant quartz-diorites and plagiogranites. Nonetheless, troctolites and gabbros are locally found within gabbronoritic series. The sheeted dike complex and the volcanic sequence include basalts, basaltic andesites, andesites, dacites and rhyolites showing both IAT (low-Ti) and boninitic (very low-Ti) affinities (Beccaluva et al., 1994; Shallo, 1994; Bortolotti et al., 1996; Bébien et al., 2000). Volcanic rocks occur as both massive and pillow lavas. Finally, the whole ophiolitic sequence is frequently cross cut by boninitic dykes.

Radiolarian cherts associated with lavas gave Bathonian to early Callovian - Bathonian to late Oxfordian ages for the WMO and EMO, respectively (Marcucci et al., 1994; Marcucci and Prella, 1996; Chiari et al., 2002). Creation of oceanic crust is inferred to have started around the Early/Middle

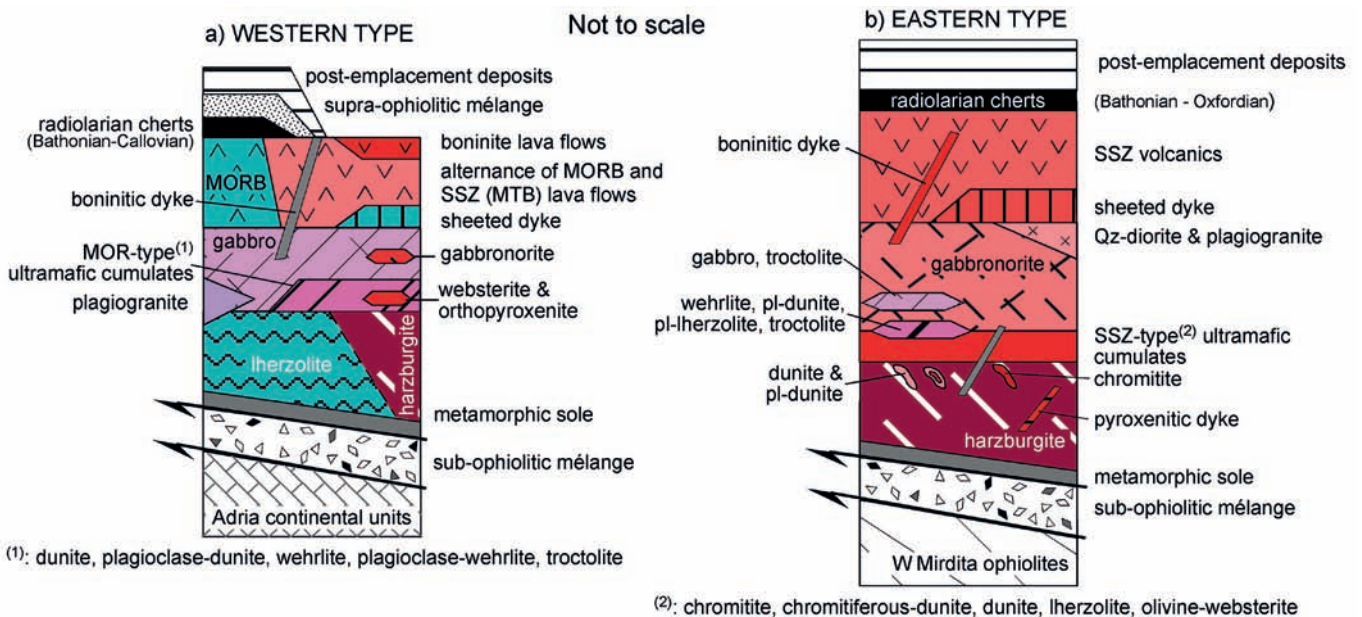


Fig. 2 - Reconstructed stratigraphic columns of the western-type (a) and eastern-type (b) Mirdita ophiolites. Compiled from: Beccaluva et al. (1994), Shallo (1994); Bébien et al. (2000); Bortolotti et al. (2002; 2013); Hoeck et al. (2002, 2014); Saccani et al. (2011).

Triassic boundary, as testified by the Triassic radiolarites associated with basalts in the sub-ophiolitic mélanges cropping out from Albania to Greece (Bortolotti et al., 2002; 2004; 2006). The intra-oceanic subduction is dated as Middle to Late Jurassic (Dilek et al., 2005; 2008). Both WMO and EMO share the same post-emplacement deposits, which include the Late Jurassic - Early Cretaceous supra-ophiolitic mélange (Simoni Mélange) and Firza Flysch and the Early-Late Cretaceous post-orogenic carbonate sequence (Bortolotti et al., 2013).

SAMPLING AND PETROGRAPHY

Western-type ophiolites

A total of five samples were selected from the WMO. One mantle lherzolite sample is taken from the Gomsiqe ultramafic massif, whereas ultramafic cumulates were collected from two separate dunite-troctolite layered series in the Skanderbeu massif (Fig. 1). Samples AL7 (dunite) and AL6 (troctolite) were collected from two adjacent layers at the mantle tectonite - ultramafic cumulate transition zone. In contrast, samples AL9 (dunite) and AL10 (troctolite) were collected from two adjacent layers at the top of the cumulitic sequence.

Mantle lherzolite sample shows porphyroclastic texture. This rock consists of olivine (65%), orthopyroxene (25%), subordinate clinopyroxene (10%) and very minor chromian spinel. Kink-banding in olivine and orthopyroxene and mutual exsolution lamellae in both pyroxenes are frequently observed. Cumulitic dunites display mesh texture, where sub-rounded, fresh relics of olivine are included in a serpentine matrix. Chromian spinel shows different size and shape, ranging from lobate to euhedral. In troctolites, olivine (~50%) and plagioclase represent the cumulus phases, whereas the intercumulus minerals are represented by plagioclase and very minor clinopyroxene (~5%). Total plagioclase is ~45% in volume.

Eastern-type ophiolites

Several samples were collected from the EMO, eighteen of which were selected based on their relatively low alteration degree and occurrence of spinels suitable for mineral chemistry analysis. A couple of samples of mantle harzburgites were taken from the Bulqiza ultramafic massif (Fig. 1), where also two samples of chromitiferous-dunites and one dunite sample were collected from dunite-chromitite pods in the uppermost part of the mantle section. One dunite, two plagioclase-dunites, and one troctolite sample were collected in the Krasta layered ultramafic series in the south Bulqiza massif, whereas one plagioclase-dunite sample was taken from the northwestern part of the Krrab massif (Fig. 1). Lherzolites, plagioclase-lherzolites, and olivine-websterites were collected from the lower cumulitic series of the Kukes and Shebenik massifs. One sample for each rock-type has been taken in both these localities.

Mantle harzburgites show well-developed porphyroclastic texture and kink banding in olivine and orthopyroxene crystals. Orthopyroxene frequently shows clinopyroxene exsolutions. Chromian spinel displays either lobate or subhedral shape. The modal amount of clinopyroxene is less than 3%. Alteration occurs to a variable extent, producing hydrated associations of serpentine minerals, chlorite, talc and opaque minerals.

Dunites, chromitiferous-dunites, and plagioclase-dunites show adcumulitic textures. In chromitiferous-dunites, coarse, subhedral chromian spinel is the cumulus phase, which is set in a serpentine matrix. Most chromian spinels exhibit fractures filled by serpentine. A few chromian spinel grains contain inclusions of serpentinized olivine. Dunites and plagioclase-dunites are characterized by sub-rounded olivine grains. In plagioclase-dunites, little amount of intercumulus plagioclase (~5-10%) is totally altered into sericite. These rocks display mesh texture, where relics of olivine are included in a serpentine matrix. Lherzolites and plagioclase-lherzolites show fine-grained, mesocumulitic texture with sub-rounded olivine grains and, when present, subhedral plagioclase, which is bigger in size compared to olivine. Orthopyroxene and clinopyroxene are subhedral in shape and often show kink banding and exsolution lamellae. The composition of intercumulus minerals cannot be estimated due to an intense alteration into chlorite. Olivine-websterites have coarse-grained, mesocumulitic texture with olivine and clinopyroxene as cumulus phases and orthopyroxene as intercumulus mineral. In some samples, clinopyroxene may reach up to 1 cm in size. Regardless of the alteration mineral assemblage, the average primary composition of these rocks is: olivine = 0-35%, clinopyroxene = 40-65%, orthopyroxene = 25-35%. Chromian spinel is a ubiquitous accessory mineral (~1-5%) in all ultramafic cumulates and occurs either as lobate intercumulus crystals or subhedral cumulus crystals. Troctolite shows orthocumulitic texture, with cumulus olivine (~60%) and intercumulus plagioclase (~40%). Chromian spinel is the accessory phase.

ANALYTICAL METHODS

Major element mineral composition was determined by electron probe microanalysis using a Cameca SX50 instrument, at IGG-CNR, Padua (Italy). Acceleration voltage and sample current were 15 keV and 20 μ A, respectively, and counting time was 100 s. Instrumental calibration was made using natural and synthetic minerals as standards. The PAP method for matrix correction (Pouchou and Pichoir, 1985) was applied. Analytical precision was better than $\pm 2\%$ for elements in the 10-20 wt% oxide range, better than 5% for elements in the 2-10 wt% oxide range, and better than 10% for elements in the 0.5-2 wt% oxide range. A total of 83 analyses of olivine and 97 analyses of chromian spinels has been performed. Representative analyses are listed in Tables 1 and 2.

MINERAL CHEMISTRY AND GEOTHERMOMETRY

Olivine

Western-type ophiolites

Olivines from the WMO rocks are unzoned and display a quite restricted forsterite content ranging from Fo₈₇ to Fo₉₀. Olivine from mantle lherzolite displays the highest forsterite content (Table 1). Olivines in the dunite AL7 and the associated troctolite AL6 have different forsterite contents, which are ~89% and ~87%, respectively. In contrast dunite AL9 and the associated troctolite AL10 have very similar forsterite contents, which are ranging from ~87% to ~88%. TiO₂, Al₂O₃, CaO, and NiO contents are very low in all olivines from the different rocks (Table 2).

Table 1 - Representative analyses of olivines (ol) from mantle tectonites and ultramafic cumulitic rocks from the Mirdita ophiolites.

Rock	Eastern Mirdita Ophiolites																													
	mantle harzburgite				chromitiferous-dunite				dunite				plagioclase-dunite																	
Locality	Bulqiza				Bulqiza				Krasta				Shebenik				Krrab				Krasta									
Sample	AL12	AL12	SH23	SH23	SH23	SH23	SH23	SH23	SH23	SH13	SH13	SH13	SH13	SH68	SH68	SH68	SH68	SHK1	SHK1	SKK1	SKK1	AL70	AL70	AL70	AL70	AL71	AL71	AL71	AL71	
Mineral	ol2	ol3	ol3	ol7	ol16	ol16	ol16	ol16	ol16	ol16	ol16	ol16	ol16	ol1r	ol1r	ol1r	ol1r	ol2c	ol2r	ol2r	ol2r	ol1c	ol1c	ol1c	ol1c	ol1	ol1	ol1	ol1	
SiO ₂	40.97	41.28	41.27	41.34	41.70	41.85	41.85	41.85	41.85	41.17	41.26	41.26	41.17	40.84	40.84	41.15	41.15	40.81	40.61	40.61	40.61	41.29	41.02	41.02	41.39	41.39	41.39	41.39	40.94	
TiO ₂	0.02	0.00	0.00	0.01	0.01	0.01	0.01	0.01	0.01	0.00	0.03	0.00	0.00	0.01	0.01	0.00	0.00	0.00	0.00	0.00	0.00	0.00	0.00	0.00	0.01	0.01	0.01	0.01	0.00	
Al ₂ O ₃	0.00	0.01	0.00	0.00	0.00	0.01	0.01	0.01	0.01	0.03	0.00	0.00	0.03	0.00	0.00	0.00	0.00	0.00	0.00	0.00	0.00	0.00	0.01	0.01	0.01	0.00	0.00	0.00	0.00	
Cr ₂ O ₃	0.01	0.00	0.00	0.02	0.01	0.03	0.03	0.03	0.03	0.02	0.04	0.03	0.02	0.03	0.03	0.03	0.03	0.00	0.00	0.00	0.00	0.05	0.04	0.04	0.04	0.04	0.04	0.00	0.00	
FeO	8.74	8.58	9.20	9.13	5.21	5.66	5.66	5.66	5.66	7.69	7.09	7.09	7.69	8.05	8.05	7.53	7.53	8.99	9.73	9.73	9.30	9.30	9.00	9.00	8.47	8.47	8.47	9.10	9.10	
MnO	0.13	0.15	0.15	0.16	0.09	0.16	0.16	0.16	0.16	0.08	0.08	0.08	0.08	0.08	0.08	0.15	0.15	0.13	0.22	0.22	0.17	0.17	0.10	0.10	0.14	0.14	0.14	0.16	0.16	
MgO	49.78	50.20	50.09	50.34	52.57	52.59	52.59	52.59	52.59	50.64	50.99	50.99	50.64	50.23	50.23	50.93	50.93	49.46	48.62	48.62	49.84	49.69	49.69	49.69	50.47	50.47	50.47	49.32	49.32	
CaO	0.01	0.01	0.02	0.02	0.16	0.16	0.16	0.16	0.16	0.02	0.02	0.02	0.02	0.04	0.04	0.02	0.02	0.04	0.01	0.01	0.04	0.03	0.03	0.03	0.04	0.04	0.04	0.05	0.05	
Na ₂ O	0.00	0.01	0.00	0.00	0.02	0.00	0.00	0.00	0.00	0.00	0.00	0.00	0.00	0.00	0.00	0.00	0.00	0.00	0.02	0.02	0.02	0.00	0.01	0.01	0.00	0.00	0.00	0.01	0.01	
NiO	0.40	0.41	0.00	0.00	0.51	0.38	0.38	0.38	0.38	0.38	0.44	0.44	0.38	0.00	0.00	0.00	0.00	0.34	0.47	0.47	0.39	0.36	0.36	0.36	0.33	0.33	0.33	0.42	0.42	
Total	100.06	100.65	100.77	100.92	100.28	100.85	100.85	100.85	100.85	100.22	99.63	99.91	100.03	99.28	99.28	99.81	99.81	99.77	99.68	99.68	101.07	100.25	100.25	100.89	100.89	100.89	100.00	100.00	100.00	
Si	1.000	1.000	1.000	0.999	1.000	0.999	0.999	0.999	0.999	0.999	0.999	1.001	1.000	0.999	0.999	0.999	0.999	1.000	1.000	1.000	1.000	1.000	1.000	1.000	1.000	1.000	1.000	1.001	1.001	
Ti	0.000	0.000	0.000	0.000	0.000	0.000	0.000	0.000	0.000	0.000	0.001	0.000	0.000	0.000	0.000	0.000	0.000	0.000	0.000	0.000	0.000	0.000	0.000	0.000	0.000	0.000	0.000	0.000	0.000	
Al	0.000	0.000	0.000	0.000	0.000	0.000	0.000	0.000	0.000	0.000	0.000	0.000	0.001	0.000	0.000	0.000	0.000	0.000	0.000	0.000	0.000	0.000	0.000	0.000	0.000	0.000	0.000	0.000	0.000	
Cr	0.000	0.000	0.000	0.000	0.000	0.000	0.000	0.000	0.000	0.002	0.001	0.001	0.000	0.001	0.001	0.001	0.001	0.000	0.000	0.000	0.000	0.000	0.000	0.000	0.000	0.000	0.000	0.000	0.000	
Fe ²⁺	0.178	0.174	0.186	0.185	0.104	0.113	0.113	0.113	0.113	0.185	0.180	0.144	0.156	0.165	0.165	0.153	0.153	0.184	0.200	0.200	0.188	0.188	0.183	0.183	0.171	0.171	0.171	0.186	0.186	
Mn	0.003	0.003	0.003	0.003	0.002	0.003	0.003	0.003	0.003	0.001	0.003	0.002	0.002	0.002	0.002	0.003	0.003	0.003	0.003	0.005	0.005	0.003	0.003	0.002	0.003	0.003	0.003	0.003	0.003	
Mg	1.811	1.813	1.810	1.813	1.879	1.872	1.872	1.872	1.872	1.805	1.810	1.843	1.833	1.832	1.832	1.844	1.844	1.806	1.785	1.785	1.799	1.799	1.805	1.805	1.817	1.817	1.817	1.798	1.798	
Ca	0.000	0.000	0.001	0.000	0.004	0.004	0.004	0.004	0.004	0.002	0.002	0.001	0.001	0.001	0.001	0.001	0.001	0.001	0.000	0.000	0.000	0.001	0.001	0.001	0.001	0.001	0.001	0.001	0.001	
Na	0.000	0.000	0.000	0.000	0.001	0.000	0.000	0.000	0.000	0.000	0.000	0.000	0.000	0.000	0.000	0.000	0.000	0.000	0.000	0.000	0.000	0.000	0.000	0.000	0.000	0.000	0.000	0.000	0.000	
Ni	0.008	0.008	0.000	0.000	0.010	0.007	0.007	0.007	0.007	0.006	0.005	0.009	0.007	0.000	0.000	0.000	0.000	0.007	0.009	0.009	0.008	0.008	0.007	0.007	0.006	0.006	0.006	0.008	0.008	
Total	3.000	3.000	3.000	3.001	3.000	3.000	3.000	3.000	3.000	3.000	3.000	2.999	3.000	3.000	3.000	3.000	3.000	3.000	3.000	3.000	3.000	3.000	3.000	3.000	3.000	3.000	3.000	2.999	2.999	
Fo (%)	90.9	91.1	90.5	90.6	94.6	94.1	94.1	94.1	94.1	90.6	90.8	92.7	92.1	91.7	92.1	92.1	92.1	90.7	89.7	89.7	90.4	90.7	90.4	90.7	91.3	91.3	90.4	90.4	90.4	
Fa (%)	8.9	8.7	9.3	9.2	5.3	5.7	5.7	5.7	5.7	9.3	9.0	7.2	7.8	8.2	7.7	7.7	7.7	9.2	10.1	10.1	9.4	9.2	9.4	9.2	8.6	8.6	9.4	9.4	9.4	
Teph (%)	0.1	0.2	0.2	0.2	0.1	0.2	0.2	0.2	0.2	0.1	0.2	0.1	0.1	0.1	0.2	0.2	0.2	0.1	0.2	0.2	0.2	0.2	0.2	0.1	0.1	0.1	0.2	0.2	0.2	
Mg#	0.91	0.91	0.91	0.91	0.95	0.94	0.94	0.94	0.94	0.91	0.91	0.93	0.92	0.92	0.92	0.92	0.92	0.91	0.90	0.90	0.91	0.91	0.91	0.91	0.91	0.91	0.91	0.91	0.91	
Mg# (melt):	-	-	-	-	0.85	0.86	0.86	0.86	0.86	0.76	0.77	0.78	0.78	0.79	0.79	0.79	0.79	0.74	0.74	0.74	0.76	0.76	0.76	0.76	0.77	0.77	0.77	0.77	0.77	0.77
0.5 GPa	-	-	-	-	0.85	0.86	0.86	0.86	0.86	0.76	0.77	0.78	0.78	0.79	0.79	0.79	0.79	0.74	0.74	0.74	0.76	0.76	0.76	0.76	0.77	0.77	0.77	0.77	0.77	0.77
1.0 GPa	-	-	-	-	0.85	0.86	0.86	0.86	0.86	0.76	0.77	0.78	0.78	0.79	0.79	0.79	0.79	0.74	0.74	0.74	0.76	0.76	0.76	0.76	0.77	0.77	0.77	0.77	0.77	0.77

Abbreviations, Fo- forsterite; Fa- fayalite; Teph: tephrolite. Mg# = Mg/(Mg+Fe²⁺). Calculated Mg# in the parental melt (after Ulmer, 1989) for pressures of 0.5 and 1.0 GPa are also reported (see text for explanation).

Table 1 (*continues*)

Rock	Eastern Mirdita Ophiolites												troctolite				
	Iherzolite			plagioclase-Iherzolite			olivine-websterite			Krasta							
	Kukes	Shebenik		Kukes	Shebenik		Shebenik	Kukes									
Locality	SH52E ol2r	SH52E ol3c	SH75 ol1	SH4198 ol1c	SH4198 ol3c	SH4198 ol2r	SH63 ol1	SH63 ol2	SH63 ol3	SH72 ol1c	SH72 ol1r	SH72 ol2	SH72 ol3	SH46E1 ol1	SH46E1 ol2	AL73 ol3	AL73 ol4
Sample	40.06	40.15	40.58	39.21	39.54	39.30	40.67	40.51	40.59	40.03	39.97	40.21	40.05	40.09	40.42	40.48	40.88
Mineral	0.00	0.00	0.02	0.00	0.00	0.00	0.00	0.00	0.03	0.01	0.00	0.01	0.00	0.02	0.00	0.03	0.01
	0.01	0.00	0.01	0.00	0.00	0.00	0.00	0.00	0.00	0.01	0.00	0.00	0.00	0.00	0.00	0.04	0.00
	0.00	0.00	0.00	0.00	0.00	0.00	0.01	0.00	0.00	0.01	0.07	0.00	0.00	0.00	0.00	0.10	0.03
	11.81	11.01	12.30	19.30	18.85	19.83	9.61	9.53	9.87	15.16	14.92	14.87	15.32	12.94	13.36	12.14	11.42
	0.21	0.21	0.16	0.28	0.23	0.28	0.15	0.20	0.14	0.31	0.31	0.26	0.24	0.15	0.20	0.21	0.22
	46.92	47.44	47.28	41.52	42.04	41.35	48.96	48.78	48.84	44.97	45.01	45.34	45.03	46.29	46.52	47.33	48.15
	0.03	0.01	0.02	0.00	0.01	0.00	0.03	0.01	0.02	0.03	0.01	0.00	0.03	0.00	0.01	0.05	0.01
	0.00	0.01	0.00	0.00	0.00	0.00	0.00	0.00	0.00	0.00	0.00	0.00	0.01	0.00	0.00	0.00	0.00
	0.16	0.13	0.30	0.20	0.31	0.21	0.00	0.00	0.00	0.18	0.22	0.18	0.13	0.23	0.25	0.31	0.31
Total	99.20	98.96	100.67	100.51	100.98	100.97	99.44	99.03	99.49	100.71	100.51	100.87	100.81	99.72	100.76	100.68	101.03
Si	1.000	1.000	1.000	1.000	1.001	1.000	1.001	1.001	1.000	0.999	0.999	1.000	0.999	1.000	1.000	0.997	1.000
Ti	0.000	0.000	0.000	0.000	0.000	0.000	0.000	0.000	0.001	0.000	0.000	0.000	0.000	0.000	0.000	0.001	0.000
Al	0.000	0.000	0.000	0.000	0.000	0.000	0.000	0.000	0.000	0.000	0.000	0.000	0.000	0.000	0.000	0.001	0.000
Cr	0.000	0.000	0.000	0.000	0.000	0.000	0.000	0.000	0.000	0.000	0.001	0.000	0.000	0.000	0.000	0.002	0.001
Fe ²⁺	0.246	0.229	0.253	0.412	0.399	0.422	0.198	0.197	0.203	0.316	0.312	0.309	0.320	0.270	0.276	0.250	0.234
Min	0.004	0.004	0.003	0.006	0.005	0.006	0.003	0.004	0.003	0.007	0.007	0.005	0.005	0.003	0.004	0.004	0.005
Mg	1.745	1.762	1.736	1.578	1.587	1.568	1.796	1.797	1.793	1.673	1.677	1.681	1.674	1.721	1.715	1.738	1.755
Ca	0.001	0.000	0.001	0.000	0.000	0.000	0.001	0.000	0.001	0.001	0.000	0.000	0.001	0.000	0.000	0.001	0.000
Na	0.000	0.000	0.000	0.000	0.000	0.000	0.000	0.000	0.000	0.000	0.000	0.000	0.000	0.000	0.000	0.000	0.000
Ni	0.003	0.003	0.006	0.004	0.006	0.004	0.000	0.000	0.000	0.004	0.004	0.004	0.003	0.005	0.005	0.006	0.006
Total	3.000	3.000	3.000	3.000	2.999	3.000	2.999	2.999	3.000	3.000	3.000	3.000	3.001	3.000	3.000	3.001	3.000
Fo (%)	87.4	88.3	87.1	79.1	79.7	78.6	89.9	89.9	89.7	83.8	84.0	84.2	83.8	86.3	85.9	87.2	88.1
Fa (%)	12.3	11.5	12.7	20.6	20.0	21.1	9.9	9.9	10.2	15.9	15.6	15.5	16.0	13.5	13.8	12.6	11.7
Teph (%)	0.2	0.2	0.1	0.3	0.2	0.3	0.2	0.2	0.1	0.3	0.3	0.3	0.3	0.2	0.2	0.2	0.2
Mg#	0.88	0.88	0.87	0.79	0.80	0.79	0.90	0.90	0.90	0.84	0.84	0.84	0.84	0.86	0.86	0.87	0.88
Mg# (melt):																	
0.5 GPa	0.70		0.69	0.57	0.57		0.74	0.74		0.63	0.63	0.63		0.65		0.68	
1.0 GPa	0.71		0.71	0.59	0.59		0.75	0.75		0.64	0.64	0.64		0.66		0.70	

Table 1 (continues)

Rock	Western Mirdita Ophiolites									
	mantle lherzolite		dunite				troctolite			
	Gomsiqe		Skanderbeu				Skanderbeu			
Locality										
Sample	AL28	AL28	AL7	AL7	AL9	AL9	AL6	AL6	AL10	AL10
Mineral	ol 1c	ol 1r	ol 3	ol 4	ol 2c	ol 2r	ol 1	ol 3	ol 1	ol 4
SiO ₂	40.89	40.85	41.00	41.11	40.77	40.84	40.54	40.60	40.49	41.11
TiO ₂	0.03	0.01	0.00	0.00	0.00	0.00	0.01	0.00	0.00	0.00
Al ₂ O ₃	0.00	0.00	0.01	0.00	0.00	0.00	0.09	0.02	0.02	0.02
Cr ₂ O ₃	0.05	0.00	0.01	0.03	0.02	0.00	0.00	0.00	0.00	0.01
FeO	9.86	9.91	10.23	10.24	11.16	11.77	11.71	11.98	11.63	11.31
MnO	0.17	0.21	0.21	0.19	0.13	0.13	0.21	0.20	0.17	0.16
MgO	48.97	48.93	48.98	49.08	48.11	47.99	47.59	47.56	47.60	48.59
CaO	0.03	0.00	0.17	0.19	0.03	0.04	0.03	0.04	0.02	0.04
Na ₂ O	0.02	0.00	0.00	0.00	0.02	0.00	0.02	0.00	0.00	0.00
NiO	0.40	0.44	0.00	0.00	0.24	0.19	0.30	0.30	0.26	0.20
Total	100.42	100.35	99.71	100.84	100.48	100.96	100.49	100.70	100.19	101.43
Si	0.999	1.000	1.000	1.001	1.001	1.000	0.998	0.999	0.999	1.000
Ti	0.001	0.000	0.000	0.000	0.000	0.000	0.000	0.000	0.000	0.000
Al	0.000	0.000	0.000	0.000	0.000	0.000	0.003	0.001	0.001	0.001
Cr	0.001	0.000	0.000	0.001	0.000	0.000	0.000	0.000	0.000	0.000
Fe ²⁺	0.202	0.203	0.209	0.208	0.229	0.241	0.241	0.246	0.240	0.230
Mn	0.004	0.004	0.004	0.004	0.003	0.003	0.004	0.004	0.004	0.003
Mg	1.784	1.785	1.781	1.781	1.760	1.752	1.747	1.744	1.751	1.761
Ca	0.001	0.000	0.004	0.005	0.001	0.001	0.001	0.001	0.001	0.001
Na	0.001	0.000	0.000	0.000	0.001	0.000	0.001	0.000	0.000	0.000
Ni	0.008	0.009	0.000	0.000	0.005	0.004	0.006	0.006	0.005	0.004
Total	3.000	3.000	3.000	2.999	3.000	3.000	3.001	3.001	3.000	3.000
Fo (%)	89.7	89.6	89.3	89.3	88.4	87.8	87.7	87.4	87.8	88.3
Fa (%)	10.1	10.2	10.5	10.5	11.5	12.1	12.1	12.4	12.0	11.5
Teph (%)	0.2	0.2	0.2	0.2	0.1	0.1	0.2	0.2	0.2	0.2
Mg#	0.90	0.90	0.90	0.90	0.88	0.88	0.88	0.88	0.88	0.88
Mg# (melt):										
0.5 GPa	-		0.73		0.69		0.69		0.69	
1.0 GPa	-		0.74		0.71		0.70		0.71	

Eastern-type ophiolites

Olivines from the EMO rocks are generally unzoned and show a wide range of forsterite content. Olivines from mantle harzburgites ranges from Fo_{90.5} to Fo_{91.1}. Olivines compositions in chromitiferous-dunite are characterized by high MgO contents and vary in composition from Fo_{94.2} to Fo_{94.7}. Also in dunites, olivines generally display high forsterite contents, which range from Fo_{91.6} to Fo_{92.7}. However, dunite AL75 (Krasta series) and plagioclase-dunites have olivines showing comparatively lower forsterite contents, which range from Fo_{89.7} to Fo_{91.3}. Olivines in lherzolites have a quite uniform composition, ranging from Fo_{87.1} to Fo_{88.5}. In contrast, olivines in the analyzed plagioclase-lherzolites show very different compositions. In samples from the Shebenik massif they show high forsterite contents (Fo_{89.7} - Fo_{89.9}), which are similar to those of olivine in plagioclase-dunites. These forsterite contents are higher than those observed in lherzolites. However, plagioclase-lherzolite SH4198 from the Kukes massif have olivines with very low forsterite contents (Fo_{78.6} - Fo_{79.7}), which likely reflect iron mobilization due to alteration processes.

The forsterite contents in olivines from olivine-websterites decrease with respect to olivines from the above mentioned rocks. However, a significant difference in olivine composition can be observed between olivine-websterite from the Kukes massif (Fo_{85.9} - Fo_{86.3}) and that from the Shebenik massif (Fo_{83.8} - Fo_{84.2}). Finally, troctolite AL73 (Krasta series) has olivine composition (Fo_{87.2} - Fo_{88.1}) similar to that of lherzolites from the EMO, as well as to troctolites from the WMO.

The NiO content of olivine generally increases with increasing forsterite content (Table 1). There is a positive correlation between Ni in olivine and forsterite content although this correlation shows a very smooth slope on a forsterite-NiO plot (not shown). Nonetheless, there are some exceptions to this general tendency. Olivine in plagioclase-lherzolite SH4198 (Kukes massif) shows high NiO contents (0.19 - 0.33 wt%) in relation to the forsterite content. This is probably a consequence of an increase in iron due to alteration processes. In contrast, olivines in lherzolite SH52E (Kukes massif) have low NiO contents (0.09 - 0.18 wt%) in relation to the forsterite content.

Table 2 (continues)

Rock		Eastern Mirdita Ophiolites																										
		dunite						plagioclase-dunite						Iherzolite						plagioclase-Iherzolite								
		Shebenik			Krrab			Krastra			Kukes			Shebenik			Kukes			Shebenik			Kukes					
Locality	SH68	SH68	SHK1	AL70	AL70	AL71	AL71	AL71	AL71	AL71	AL71	AL71	SH52E	SH52E	SH75	SH75	SH75	SH75	SH75	SH75	SH75	SH75	SH4198	SH4198	SH63	SH63	SH63	
Sample	sp 2c	sp 2r	sp 1	sp 1	sp 2	sp 1	sp 1	sp 3	sp 4	sp 1	sp 1	sp 1	sp 1c	sp 1r	sp 1c	sp 1r	sp 1r	sp 1c	sp 1r	sp 2c	sp 2r	sp 4c	sp 4r	sp 1r	sp 1c	sp 1r	sp 1r	
Mineral																												
TiO ₂	0.13	0.13	0.52	0.22	0.20	0.17	0.06	0.12	0.12	0.14	0.09	0.09	0.14	0.09	0.09	0.11	0.11	0.14	0.14	0.11	0.14	0.63	0.66	0.99	0.99	1.17	1.17	1.17
Al ₂ O ₃	9.26	9.39	27.98	31.49	30.95	31.95	34.65	36.21	36.21	18.07	20.68	17.15	18.30	17.14	18.60	17.14	18.60	17.14	18.60	17.14	18.60	25.24	19.32	20.71	20.71	20.74	20.74	20.74
Cr ₂ O ₃	60.23	59.89	33.70	35.62	35.72	34.34	32.43	29.27	29.27	49.18	46.33	49.35	47.42	48.57	47.40	48.57	47.40	48.57	47.40	48.57	47.40	25.75	31.16	40.54	39.97	39.97	39.97	39.97
FeO	22.59	21.94	25.66	17.65	17.26	17.46	16.86	18.36	18.36	22.47	22.09	24.04	24.15	24.56	25.20	24.56	25.20	24.04	24.15	24.56	25.20	36.90	39.03	25.93	26.22	26.22	26.22	26.22
MnO	0.00	0.00	0.00	0.00	0.00	0.00	0.00	0.00	0.00	0.00	0.00	0.00	0.00	0.00	0.00	0.00	0.00	0.00	0.00	0.00	0.00	0.00	0.00	0.11	0.11	0.00	0.00	0.00
MgO	8.68	8.97	10.72	14.78	14.48	14.68	15.35	14.68	14.68	8.89	9.64	8.52	8.81	8.29	8.23	8.29	8.23	8.52	8.81	8.29	8.23	9.26	8.02	10.47	10.60	10.60	10.60	10.60
NiO	0.00	0.00	0.16	0.12	0.14	0.22	0.14	0.10	0.10	0.00	0.03	0.12	0.11	0.04	0.00	0.04	0.00	0.12	0.11	0.04	0.00	0.09	0.08	0.02	0.02	0.02	0.02	0.02
Total	100.89	100.32	98.73	99.88	98.75	98.82	99.50	98.73	98.73	98.75	98.86	99.27	98.90	98.71	99.58	98.71	99.58	98.90	98.71	99.58	99.58	97.87	98.27	98.77	98.77	98.77	98.77	98.77
Fe ₂ O ₃	2.10	2.05	6.17	3.46	3.07	3.54	3.33	3.73	3.73	1.54	1.97	2.79	3.29	3.06	3.04	3.06	3.04	3.29	3.06	3.06	3.04	16.60	17.68	6.80	7.05	7.05	7.05	7.05
FeO	20.70	20.10	20.10	14.53	14.50	14.27	13.86	15.00	15.00	21.08	20.32	21.53	21.19	21.80	22.46	21.80	22.46	21.53	21.19	21.80	22.46	21.96	23.12	19.81	19.88	19.88	19.88	19.88
Total	101.10	100.53	99.35	100.23	99.06	99.17	99.83	99.10	99.10	98.90	99.06	99.55	99.23	99.02	99.88	99.02	99.88	99.55	99.23	99.02	99.88	99.53	100.04	99.45	99.43	99.43	99.43	99.43
Ti	0.003	0.003	0.012	0.005	0.004	0.004	0.001	0.003	0.003	0.003	0.002	0.002	0.003	0.003	0.003	0.003	0.003	0.002	0.003	0.003	0.003	0.015	0.016	0.024	0.024	0.028	0.028	0.028
Al	0.362	0.368	1.014	1.088	1.084	1.112	1.182	1.241	1.241	0.692	0.779	0.658	0.699	0.662	0.708	0.662	0.708	0.658	0.699	0.662	0.708	0.936	0.738	0.774	0.775	0.775	0.775	0.775
Cr	1.579	1.574	0.819	0.826	0.839	0.802	0.742	0.673	0.673	1.263	1.170	1.269	1.215	1.257	1.211	1.257	1.211	1.269	1.215	1.257	1.211	0.641	0.799	1.016	1.001	1.001	1.001	1.001
Fe ³⁺	0.052	0.051	0.143	0.076	0.069	0.078	0.073	0.082	0.082	0.038	0.047	0.068	0.080	0.075	0.074	0.075	0.074	0.068	0.080	0.075	0.074	0.393	0.431	0.162	0.168	0.168	0.168	0.168
Fe ²⁺	0.574	0.559	0.517	0.356	0.360	0.353	0.336	0.365	0.365	0.573	0.543	0.586	0.574	0.597	0.607	0.597	0.607	0.586	0.574	0.597	0.607	0.578	0.627	0.525	0.527	0.527	0.527	0.527
Min	0.000	0.000	0.000	0.000	0.000	0.000	0.000	0.000	0.000	0.000	0.000	0.000	0.000	0.000	0.000	0.000	0.000	0.000	0.000	0.000	0.000	0.000	0.000	0.000	0.000	0.000	0.000	0.000
Mg	0.429	0.444	0.491	0.646	0.641	0.646	0.662	0.636	0.636	0.430	0.459	0.413	0.426	0.405	0.396	0.405	0.396	0.413	0.426	0.405	0.396	0.434	0.388	0.495	0.501	0.501	0.501	0.501
Ni	0.000	0.000	0.004	0.003	0.003	0.005	0.003	0.002	0.002	0.000	0.001	0.003	0.003	0.001	0.000	0.001	0.000	0.003	0.003	0.001	0.000	0.002	0.002	0.002	0.001	0.001	0.001	0.001
Total	3.000	3.000	3.000	3.000	3.000	3.000	3.000	3.000	3.000	3.000	3.000	3.000	3.000	3.000	3.000	3.000	3.000	3.000	3.000	3.000	3.000	3.000	3.000	3.000	3.000	3.000	3.000	3.000
Mg#	0.43	0.44	0.49	0.65	0.64	0.65	0.66	0.64	0.64	0.43	0.46	0.41	0.43	0.40	0.40	0.40	0.40	0.41	0.43	0.40	0.40	0.43	0.38	0.49	0.49	0.49	0.49	0.49
Cr#	0.81	0.81	0.45	0.43	0.44	0.42	0.39	0.35	0.35	0.65	0.60	0.66	0.64	0.66	0.63	0.66	0.63	0.66	0.64	0.66	0.63	0.41	0.52	0.57	0.56	0.56	0.56	0.56
TiO ₂ (melt)	0.22	0.22	1.05	0.61	0.58	0.52	0.27	0.41	0.41	0.23	0.17	0.17	0.19	0.19	0.24	0.19	0.24	0.17	0.19	0.19	0.24	1.19	1.23	1.58	1.76	1.76	1.76	1.76
Al ₂ O ₃ (melt)*	10.02	10.08	15.83	16.62	16.50	16.72	17.29	17.61	17.61	13.21	13.97	12.93	13.28	12.93	13.37	12.93	13.37	12.93	13.28	12.93	13.37	15.17	13.58	13.98	13.99	13.99	13.99	13.99
Al ₂ O ₃ (melt)**	10.56	10.64	15.76	16.20	16.14	16.26	16.58	16.75	16.75	14.05	14.76	14.03	14.25	14.03	14.30	14.03	14.30	14.03	14.25	14.03	14.30	15.80	14.40	14.76	14.77	14.77	14.77	14.77
FeO/MgO(melt)	1.78	1.68	1.94	1.08	1.10	1.08	1.04	1.21	1.21	2.12	1.97	2.20	2.13	2.29	2.44	2.29	2.44	2.20	2.13	2.29	2.44	2.17	2.34	1.71	1.71	1.71	1.71	1.71

Table 2 (continues)

Rock	Eastern Mirdita Ophiolites										Western Mirdita Ophiolites																		
	olivine-websterite					troctolite					mantle lherzolite					dunite					troctolite								
	Kukes		Shebenik			AL73		AL73			AL28		AL28			AL7		AL7			AL6		AL6			AL10		AL10	
Locality	sp 1c	sp 1r	sp 1	sp 2	sp 3	sp 1	sp 2	sp 3	sp 1	sp 2	sp 1	sp 2	sp 1c	sp 1r	sp 2c	sp 1c	sp 1r	sp 2c	sp 2r	sp 2c	sp 2r	sp 3c	sp 2c	sp 2r	sp 3c	sp 2c	sp 2r	sp 3c	
Sample	SH46E1	SH46E1	SH72	SH72	AL73	AL73	AL73	AL73	AL28	AL28	AL28	AL28	AL7	AL7	AL7	AL7	AL7	AL7	AL9	AL9	AL9	AL6	AL6	AL6	AL6	AL10	AL10	AL10	AL10
Mineral	sp 1c	sp 1r	sp 1	sp 1	sp 3	sp 1	sp 2	sp 3	sp 1	sp 2	sp 1	sp 2	sp 1c	sp 1r	sp 2c	sp 1c	sp 1r	sp 2c	sp 2r	sp 2c	sp 2r	sp 3c	sp 2c	sp 2r	sp 3c	sp 2c	sp 2r	sp 3c	sp 2r
TiO ₂	0.18	0.12	0.07	0.57	0.63	0.60	0.04	0.05	0.05	0.04	0.05	0.04	0.37	0.22	0.31	0.37	0.22	0.31	0.73	0.57	0.73	0.24	0.18	0.18	0.31	1.18	0.67	0.67	0.67
Al ₂ O ₃	13.99	14.43	39.42	23.68	23.58	23.75	51.65	51.65	51.93	51.93	51.65	51.93	47.83	48.10	44.92	47.83	48.10	44.92	35.06	34.81	35.06	34.93	36.53	36.53	41.92	23.71	26.32	26.32	26.32
Cr ₂ O ₃	50.75	51.46	23.56	39.06	38.63	39.45	13.37	13.37	14.55	14.55	13.37	14.55	20.30	20.52	19.67	20.30	20.52	19.67	27.82	28.47	27.82	30.90	29.60	29.60	23.01	35.22	34.35	34.35	34.35
FeO	27.62	27.29	24.86	25.16	25.96	25.27	18.20	18.20	16.92	16.92	18.20	16.92	15.51	15.52	16.19	15.51	15.52	16.19	22.24	21.84	22.24	20.90	20.13	20.13	19.61	29.10	27.63	27.63	27.63
MnO	0.00	0.00	0.00	0.00	0.00	0.00	0.00	0.00	0.00	0.00	0.00	0.00	0.17	0.19	0.18	0.17	0.19	0.18	0.00	0.00	0.00	0.29	0.29	0.29	0.18	0.31	0.35	0.35	0.35
MgO	7.02	6.97	11.56	10.37	9.94	9.80	17.20	17.20	16.62	16.62	17.20	16.62	17.21	16.99	17.34	17.21	16.99	17.34	12.83	12.56	12.83	13.32	13.84	13.84	15.30	9.73	10.28	10.28	10.28
NiO	0.00	0.00	0.05	0.16	0.17	0.12	0.00	0.00	0.00	0.00	0.00	0.00	0.00	0.00	0.00	0.00	0.00	0.00	0.15	0.14	0.15	0.15	0.10	0.10	0.17	0.14	0.11	0.11	0.11
Total	99.56	100.27	99.52	99.00	98.91	98.99	100.47	100.47	100.06	100.06	100.47	100.06	101.28	101.54	98.61	101.28	101.54	98.61	98.83	98.39	98.83	100.73	100.67	100.67	100.50	99.37	99.70	99.70	99.70
Fe ₂ O ₃	4.41	3.71	4.79	5.64	5.81	4.74	4.48	4.48	2.23	2.23	4.48	2.23	1.91	1.48	4.28	1.91	1.48	4.28	4.50	3.96	4.50	4.01	3.79	3.79	4.61	8.45	7.78	7.78	7.78
FeO	23.65	23.95	20.55	20.08	20.74	21.01	14.16	14.16	14.92	14.92	14.16	14.92	13.79	14.19	12.34	13.79	14.19	12.34	18.19	18.28	18.19	17.29	16.72	16.72	15.46	21.49	20.62	20.62	20.62
Total	100.00	100.64	100.00	99.56	99.49	99.46	100.92	100.92	100.28	100.28	100.92	100.28	101.47	101.69	99.04	101.47	101.69	99.04	99.28	98.79	99.28	101.13	101.05	101.05	100.96	100.22	100.48	100.48	100.48
Ti	0.004	0.003	0.002	0.013	0.015	0.014	0.001	0.001	0.001	0.001	0.001	0.001	0.005	0.005	0.006	0.005	0.005	0.006	0.016	0.013	0.016	0.005	0.004	0.004	0.006	0.028	0.016	0.016	0.016
Al	0.548	0.561	1.351	0.874	0.873	0.880	1.626	1.626	1.644	1.644	1.626	1.644	1.518	1.525	1.467	1.518	1.525	1.467	1.219	1.218	1.219	1.194	1.238	1.238	1.381	0.874	0.955	0.955	0.955
Cr	1.333	1.341	0.541	0.967	0.960	0.980	0.282	0.282	0.309	0.309	0.282	0.309	0.432	0.436	0.431	0.432	0.436	0.431	0.649	0.668	0.649	0.708	0.673	0.673	0.509	0.871	0.836	0.836	0.836
Fe ³⁺	0.110	0.092	0.105	0.133	0.137	0.112	0.090	0.090	0.045	0.045	0.090	0.045	0.039	0.030	0.089	0.039	0.030	0.089	0.100	0.088	0.100	0.088	0.082	0.082	0.097	0.199	0.180	0.180	0.180
Fe ²⁺	0.657	0.660	0.500	0.526	0.545	0.552	0.316	0.316	0.335	0.335	0.316	0.335	0.311	0.319	0.286	0.311	0.319	0.286	0.449	0.454	0.449	0.419	0.402	0.402	0.361	0.562	0.530	0.530	0.530
Mn	0.000	0.000	0.000	0.000	0.000	0.000	0.000	0.000	0.000	0.000	0.000	0.000	0.004	0.004	0.004	0.004	0.004	0.004	0.000	0.000	0.000	0.007	0.007	0.007	0.004	0.008	0.009	0.009	0.009
Mg	0.348	0.342	0.501	0.484	0.465	0.459	0.685	0.685	0.666	0.666	0.685	0.666	0.691	0.681	0.716	0.691	0.681	0.716	0.564	0.556	0.564	0.575	0.593	0.593	0.637	0.454	0.471	0.471	0.471
Ni	0.000	0.000	0.001	0.004	0.004	0.003	0.000	0.000	0.000	0.000	0.000	0.000	0.000	0.000	0.000	0.000	0.000	0.000	0.004	0.003	0.004	0.003	0.002	0.002	0.004	0.003	0.003	0.003	0.003
Total	3.000	3.000	3.000	3.000	3.000	3.000	3.000	3.000	3.000	3.000	3.000	3.000	3.000	3.000	3.000	3.000	3.000	3.000	3.000	3.000	3.000	3.000	3.000	3.000	3.000	3.000	3.000	3.000	3.000
Mg#	0.35	0.34	0.50	0.48	0.46	0.45	0.68	0.68	0.67	0.67	0.68	0.67	0.69	0.68	0.72	0.69	0.68	0.72	0.56	0.55	0.56	0.58	0.60	0.60	0.64	0.45	0.47	0.47	0.47
Cr#	0.71	0.71	0.29	0.53	0.52	0.53	0.15	0.15	0.16	0.16	0.15	0.16	0.22	0.22	0.23	0.22	0.22	0.23	0.35	0.35	0.35	0.37	0.35	0.35	0.27	0.50	0.47	0.47	0.47
TiO ₂ (melt)	0.28	0.21	0.14	1.11	1.18	1.15							0.85	0.62	0.75	0.85	0.62	0.75	1.30	1.11	1.30	0.65	0.54	0.54	0.75	1.25	0.80	0.80	0.80
Al ₂ O ₃ (melt)*	11.89	12.04	18.24	14.78	14.75	14.79							19.76	19.80	19.25	19.76	19.80	19.25	17.38	17.33	17.38	17.35	17.67	17.67	18.71	14.78	15.44	15.44	15.44
Al ₂ O ₃ (melt)**	12.72	12.88	17.09	15.15	15.13	15.15							17.89	17.92	17.63	17.89	17.92	17.63	16.62	16.59	16.62	16.61	16.78	16.78	17.34	15.15	15.53	15.53	15.53
FeO/MgO(melt)	2.73	2.82	2.22	1.86	2.00	2.08							1.12	1.17	0.95	1.12	1.17	0.95	1.66	1.71	1.66	1.50	1.43	1.43	1.29	2.09	2.09	2.09	2.09

Chromian spinel

Chromian spinels occurring in different rocks in the Albanide ophiolites show a large variation in composition (Table 1). In the Cr-Al-Fe³⁺ ternary discrimination diagram (Stevens, 1944), chromian spinels from WMO rocks can be classified as Cr-spinel (*s.s.*). Moreover, spinels from ultramafic-mafic cumulates fall within the MORB compositional field (Fig. 3a, c). In contrast, spinels occurring in EMO rocks show a wide range of Cr-Al contents (Fig. 3b, c). In particular, spinels in plagioclase-dunites from the Krasta section and Krrab massif, plagioclase-lherzolites from the Kukes massif, and olivine-websterites from the Shebenik massif can be classified as Cr-spinel. In contrast, spinels from all other ultramafic-mafic cumulates can be classified as Al-chromite (Fig. 3b, c). Spinels from EMO mantle harzburgites have compositions ranging from the Cr-spinel/Al-chromite boundary to Al-chromite. Al-chromites from dunites, chromitiferous dunites, and olivine-websterites fall within or very close to the boninitic compositional field of Barnes and Roeder (2001).

The large compositional variation of the analyzed chromian spinels can also be seen in Fig. 4, which shows that all chromian spinels plot along the line representing a 1:1 replacement of Fe(Cr, Fe³⁺)₂O₄ (chromite end-member) by MgAl₂O₄ (spinel end-member). Different proportions for the two end-members can be observed in spinels from both the WMO and EMO. Mantle tectonites of both WMO and EMO have higher spinel end-member component with respect to cumulitic rocks of the same belt. The only exception is represented by plagioclase-dunites from the Krasta series (Fig. 4).

Western-type ophiolites

The restitic spinels in mantle lherzolite are very aluminous (Al₂O₃ = 51.65-51.93% and Cr# = 0.15-0.16, Fig. 5a). In the diagram in Fig. 6, they plot close to the field for abyssal peridotites. These compositional features point to low degrees of mantle melting, similar to that seen in abyssal peridotites (e.g., Dick and Bullen, 1984). Accordingly, the Cr# in spinels and Mg# in associated olivine (Fig. 7) plot within the abyssal peridotite field and indicate that these lherzolites may represent mantle residua after less than 10% melt extraction.

In dunites, individual grains are generally unzoned; the only exception is a single mineral from sample AL9. In contrast, spinels cores from troctolites are 0.90-1.30% richer in Cr₂O₃ than rim (Table 1). Interesting compositional variations can be observed in spinels from different layers in the cumulitic section of the Skanderbeu massif. Dunite AL7 and the associated troctolite AL6 have relatively high Al₂O₃ and MgO contents when compared with dunite AL9 and the associated troctolite AL10 (Table 1). For example, in dunites AL7 and AL9, Al₂O₃ content in spinel is in the range of 44.92-48.10% and 33.52-39.48%, respectively (Fig. 5a). Likewise, MgO is in the range of 16.90-17.34% in sample AL7 and 12.56-14.63% in sample AL9. The dunite AL7-troctolite AL6 pair shows much lower TiO₂ content with respect to the dunite AL9-troctolite AL10 pair (Table 1, Fig. 5b). In Fig. 5b, the dunite-troctolite pair AL9-AL10 fall within the compositional field for MORB peridotites, whereas the AL7-AL6 pair plot outside this field. Dunites and troctolites have generally low Cr# and Mg#. However, spinels in troctolite AL10 show comparatively higher Cr# and Mg# values (Table 1, Fig. 6). In particular, Cr# values of spinels in troctolite AL10 are similar to those of SSZ peridotites.

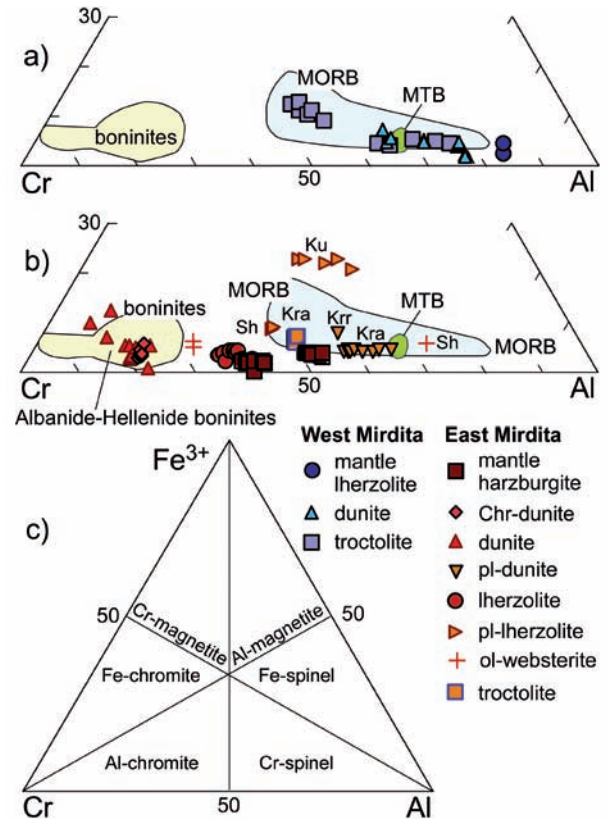


Fig. 3 - Trivalent Cr-Al-Fe³⁺ ternary cation plot of chromian spinels from the western-type (a) and eastern-type (b) mantle tectonites and ultramafic-mafic cumulates from the Miridita ophiolites, as well as nomenclature of spinels (Stevens, 1944) (c). The compositional variation of chromian spinels from mid-ocean ridge (MORB) setting (Roeder, 1994) and boninites (Barnes and Roeder, 2001), as well as boninitic basalts and medium-Ti basalts (MTB) from the Albanide-Hellenide ophiolites (O. Zeda and E. Saccani unpublished data) are shown for comparison. Abbreviations, Ku: Kukes, Krr: Krrab, Kra: Krasta, Sh: Shebenik.

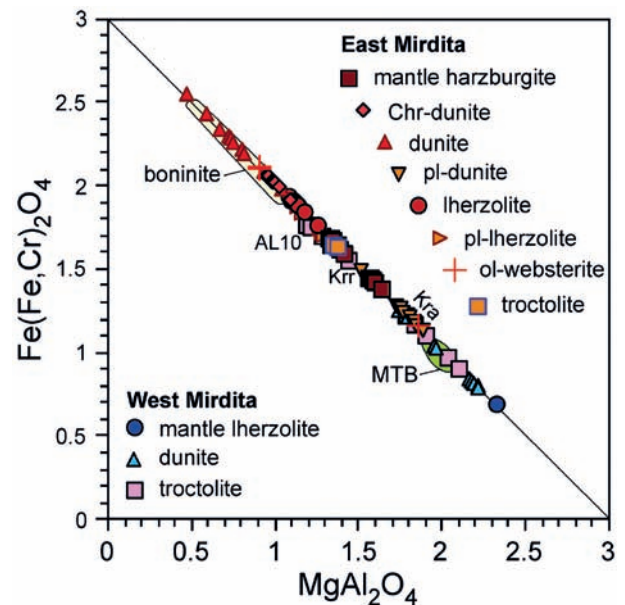


Fig. 4 - Cation plot of Cr + Fe vs. Al + Mg for chromian spinels from mantle tectonites and ultramafic cumulitic rocks from the Miridita ophiolites. The diagonal line represents a 1:1 replacement between the chromite and spinel end-members. The compositional variation of chromian spinels from boninitic basalts and medium-Ti basalts (MTB) from the Albanide-Hellenide ophiolites (O. Zeda and E. Saccani unpublished data) are shown for comparison. Abbreviations as in Fig. 3

Eastern-type ophiolites

Individual grains in both mantle harzburgites and ultramafic cumulates from the EMO commonly show compositional variation from core to rim. In most samples, spinels have cores richer in Cr_2O_3 than the rims (Table 1). In these samples, Cr_2O_3 content in core can be up to ~3% higher than in rim. However, in most dunite samples and in chromitiferous-dunites no compositional zoning is observed. In plagioclase-dunite and olivine-websterite from the Kukes massif, spinels show rims significantly richer in Cr_2O_3 (up to ~5%) than cores (Table 1).

The restitic spinels in mantle harzburgites have low Al_2O_3 contents (20.44-28.84%) and high Cr# (0.48-0.62) (Fig. 5a). Similar values are commonly associated with hydrous re-melting in the mantle wedge above a subduction zone (Dick and Bullen, 1984). In fact, the Cr# in spinels and Mg# in associated olivine (Fig. 7) plot within the SSZ peridotite field and indicate that mantle harzburgites may represent mantle residua after 20-30% melt extraction.

Spinels in dunites and chromitiferous-dunites are characterized by very low Al_2O_3 contents (~6-11.4%) and very uniform and high Cr_2O_3 content (56.8-60.5%) resulting in a

very high Cr# (Table 1 and Fig. 5a). FeO and MgO contents are variable. In Fig. 5b, as well as in the Cr# vs. Mg# plot in Fig. 6 these spinels fall within the field for boninitic chromites. Compared to dunites, spinels in plagioclase-dunites have very different compositions. They are characterized by higher Al_2O_3 (~28~36%), MgO (~11~15%) and lower Cr_2O_3 (~29~38%) contents (Fig. 5a). TiO_2 content in these spinels is generally low. Nonetheless, spinels from sample SHK1 (Krrab massif) show a rather high TiO_2 content, which is comparable to that seen in MORB-type peridotites (Table 1 and Fig. 5b). The variation of Cr# and Mg# is compatible with the composition of either abyssal or forearc peridotites (Fig. 6).

Spinels in lherzolites have chemical features typical for SSZ peridotites, that is: low Al_2O_3 (~17~21%), TiO_2 (0.09-0.14%) and high Cr_2O_3 (~46~50%) contents (Fig. 5a, b). They have Cr# and Mg# plotting in the field for SSZ peridotites in Fig. 6. In contrast, compared to lherzolites, spinels in plagioclase-lherzolites have higher Al_2O_3 and lower Cr_2O_3 contents (Fig. 5a, b). However, the most striking feature of spinels in plagioclase-lherzolites is a very high TiO_2 (0.36-1.17%) content, which is indeed similar to that observed in spinels in MORB-type peridotites (Fig. 5b). Moreover, spinels in plagioclase-lherzolite SH4198 from the Kukes massif are very rich in FeO (~37~39%), as clearly shown in Fig. 3. The high FeO contents in these spinels can be due to ferritchromitisation during cooling, serpentinisation and secondary oxidation. However, ferritchromitisation and serpentinisation should result in Fe exchange from olivine to spinel (e.g., Lee, 1999; Ahmed et al., 2001; Rollinson, 2008). Nonetheless, also the coexisting olivine shows very high FeO contents. Therefore we suggest that both olivine and spinels in this sample underwent secondary Fe-enrichment. Cr# and Mg# of spinels from the plagioclase-lherzolites of the Shebenik massif plot in the field for SSZ peridotites, whereas those from the Kukes massif plot outside this field (Fig. 6).

Spinels in olivine-websterites from the Kukes massif have very different composition with respect to those from similar rocks from the Shebenik massif. Those from the Kukes olivine-websterites have typical SSZ-type chemical features with very high Cr_2O_3 contents (Fig. 5a), as well as Cr# and TiO_2 content resembling that of boninitic spinels (Fig. 5b). Accordingly, they plot within the field for forearc peridotites in Fig. 6. By contrast, spinels from the Shebenik olivine-websterites are rich in Al_2O_3 (Table 1) and for many aspects have a general composition resembling that of spinels from MORB-type ophiolites (e.g., Fig. 3, 5a). However, they have a rather low TiO_2 content, which significantly differs from that of spinels from MORB-type ultramafic cumulates (Fig. 5b).

Spinels from the troctolite of the Krasta section are fairly rich in Cr_2O_3 (Fig. 5a) and show Cr# and Mg# resembling those of forearc peridotites (Fig. 6). Nonetheless, they have very high TiO_2 content (0.57-0.63%), which is similar to that commonly observed in MORB-type spinels (Fig. 5b).

Geothermometry

Thermometric methods should be used with some caution due to the cumulitic nature of the studied rocks, which may cause uncertainty in the recognition of co-magmatic mineral phases. For these reasons, a careful choice of minerals suitable for thermometric methods has been made. This, however, resulted in a significant reduction in the number of mineral analyses that could confidently be used.

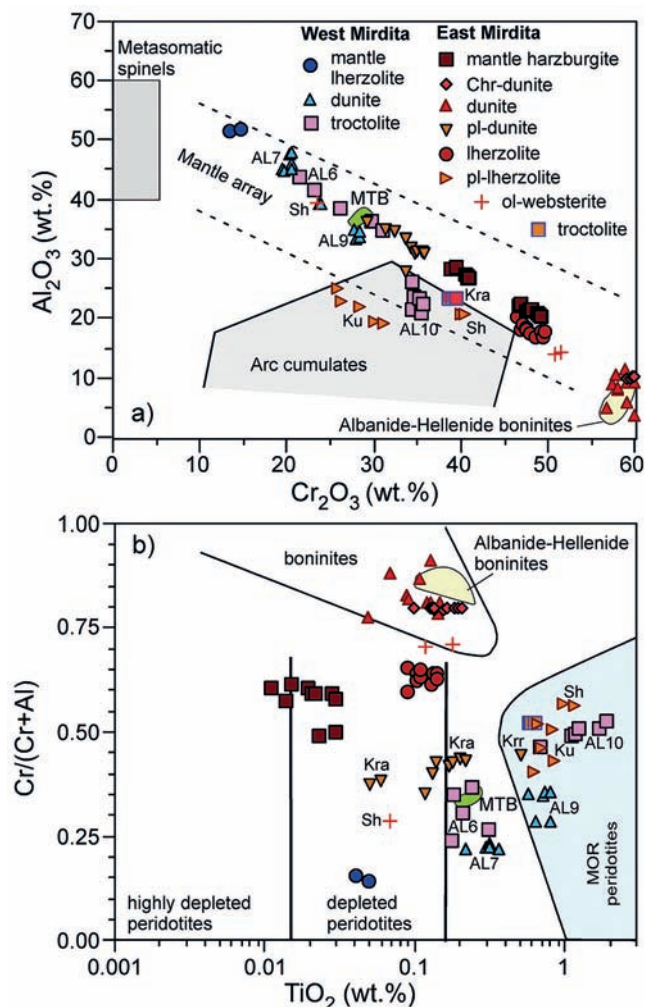


Fig. 5 - (a) Al_2O_3 vs. Cr_2O_3 (wt%) diagram (modified from Franz and Wirth, 2000) and (b) Cr# vs. TiO_2 (wt%) diagram (modified from Kepezhinskas et al., 1993) for chromian spinels from mantle tectonites and ultramafic cumulitic rocks from the Mirdita ophiolites. Compositional fields for chromian spinels in boninitic basalts and medium-Ti basalts (MTB) from the Albanide-Hellenide ophiolites (O. Zeda and E. Saccani unpublished data) are shown for comparison. Abbreviations as in Fig. 3.

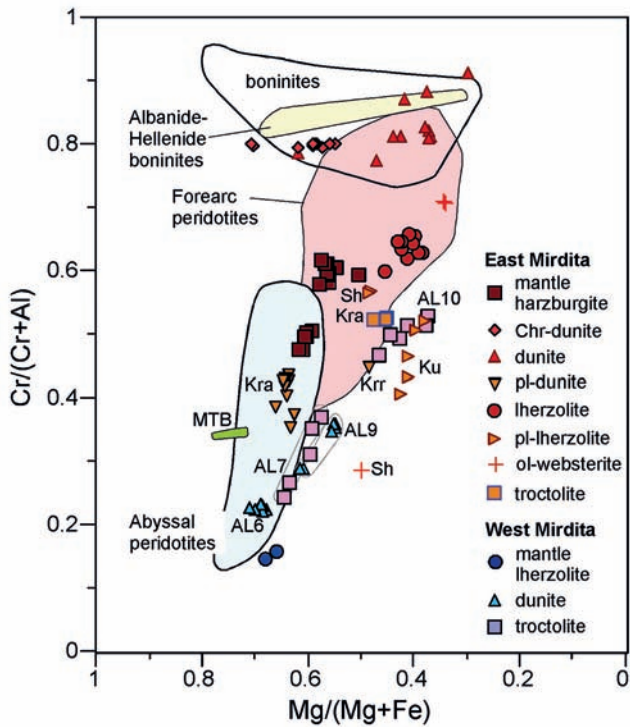


Fig. 6 - Cr# vs. Mg# diagram for chromian spinels from mantle tectonites and ultramafic cumulitic rocks from the Mirdita ophiolites (modified after Dick and Bullen, 1984). Compositional fields for spinels in boninites (Kepezhinskias et al., 1993; Barnes and Roeder, 2001), fore-arc peridotites (Parkinson and Pearce, 1998), and abyssal peridotites (Dick and Bullen, 1984), as well as Albanide-Hellenide ophiolites (O. Zeda and E. Saccani unpublished data) are shown for comparison. Abbreviations as in Fig. 3.

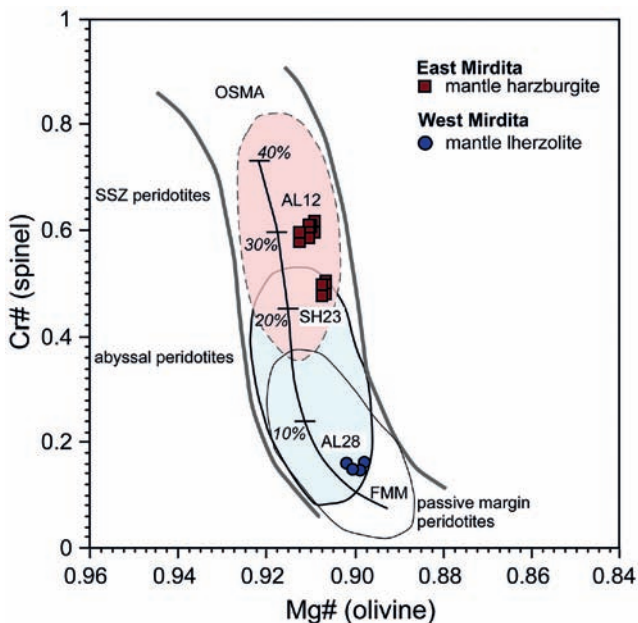


Fig. 7 - Cr#(spinel) vs. Mg#(olivine) diagram for mantle tectonites from the Mirdita ophiolites. The olivine-spinel mantle array (OSMA) and melting trend of Arai (1994). FMM = fertile MORB mantle. Compositional variations for abyssal peridotites are from Dick and Bullen (1984); compositional variations for oceanic supra-subduction zone and passive continental margin peridotites are from Pearce et al. (2000).

Cumulus minerals are only represented by olivine and chromian spinel. Therefore, the empirical calibrations of Fabriès (1979) and Ballhouse et al. (1991) were used to determine temperatures from cumulus olivine-spinel pairs. These two methods give comparable estimated temperatures, though temperatures obtained using the Ballhouse et al. (1991) thermometer systematically resulted in a few degrees lower values than those given by the Fabriès (1979) thermometer.

These thermometric methods give temperatures of 800°C and 670°C for EMO mantle harzburgites and WMO mantle lherzolite, respectively. Estimated temperatures for ultramafic-mafic cumulates from both EMO and WMO are in the range of 725°C - 810°C. No differences in estimated temperatures can be observed between different rock-types within each ophiolitic unit. All estimated temperatures are significantly lower than mantle temperatures or chromian spinel crystallization temperature (Murck and Campbell, 1986) and may indicate Fe-Mg re-equilibration during solid-state subsolidus cooling. However, Fe-Mg equilibration during cooling should result in Mg-rich rims in olivine and Fe-rich rims in chromian spinels (e.g., Rollinson, 2008). In contrast, olivines are unzoned and almost all the investigated chromian spinels do not show Fe-enrichment in rims compared to cores. Instead, chromitites in chromitiferous-dunite have rims poorer in Fe than cores (Table 2). Therefore, although these minerals experienced low-temperature re-equilibration, we infer that their composition is more likely to be original, as there is no evidence for Fe-Mg exchange between spinel and olivine.

DISCUSSION

Inferring the parental melts

Due to the cumulitic nature of the Mirdita ultramafic and mafic cumulates and the absence of any evidence of associated liquid composition (e.g., chilled margins, feeding dykes, trapped liquid, etc.), direct information about their parental magma composition is lacking. Four distinct magma-types have been recognized in the Jurassic volcanic sequences of the Mirdita ophiolites (i.e., N-MORB, MTB, IAT, and boninite; see Saccani et al., 2011, for a review). However, many authors showed that these different magma-types co-existed in both time and space and locally interacted between each other (e.g., Bortolotti et al., 1996; 2002; Bébién et al., 1997; 2000; Hoeck et al., 2002; Koller et al., 2006; Dilek et al., 2008; Saccani et al., 2011). Therefore, in many cases, genetic relationships between cumulitic rocks and any of the different magma-types cannot straightforwardly be assumed.

Nonetheless, the chemical composition of chromian spinel is a sensitive petrogenetic indicator and it has been used to constrain the parental melt composition by many authors (e.g., Dick and Bullen, 1984; Augé, 1987; Arai, 1994; Kepezhinskias et al., 1993; Zhou et al., 1996; Kamenetsky et al., 2001; Rollinson, 2008). In fact, chromian spinels occurring in cumulate rocks, as either cumulus or inter-cumulus phases, are likely to have been produced by crystallization from parental melt. Consequently, the chemical composition of chromian spinel can be used to assess parental melt composition(s). Experimental studies indicate that Al_2O_3 and TiO_2 content, as well as FeO/MgO ratios in chromian spinel are directly related to parental melt (e.g., Maurel and Maurel, 1982; Augé, 1987; Kamenetsky et al., 2001; Rollinson, 2008).

According to Maurel and Maurel (1982), the Al_2O_3 content of chromian spinel is controlled by the Al_2O_3 content of the parental melt and the latter can be calculated using the formula:

$$\text{Al}_2\text{O}_3 \text{ (wt\%)} \text{ in chromian spinel} = 0.035 \times \text{Al}_2\text{O}_3^{2.42} \text{ (wt\%)} \text{ in parental melt.}$$

By elaborating the chromian spinel data from different tectonic settings reported by Kamenetsky et al. (2001), Rollinson (2008) proposed a logarithmic expression and a power law expression that relates the Al_2O_3 content of chromian spinels and in parental melts from arc-type and MORB-type settings, respectively, as follows:

$$\text{Arc-type: } \text{Al}_2\text{O}_3 \text{ (melt)} = 5.2181 \times \text{Ln}(\text{Al}_2\text{O}_3 \text{ in spinel}) - 1.0505$$

$$\text{MORB-type: } \text{Al}_2\text{O}_3 \text{ (melt)} = 7.1518 \times \text{Al}_2\text{O}_3 \text{ (in spinel)}^{0.387}$$

Rollinson (2008) also proposed a couple of power law expressions that relates TiO_2 content in chromian spinels and in parental melt from arc-type and MORB-type settings:

$$\text{Arc-type: } \text{TiO}_2 \text{ (melt)} = 1.0963 \times \text{TiO}_2 \text{ (spinel)}^{0.7863}$$

$$\text{MORB-type: } \text{TiO}_2 \text{ (melt)} = 1.5907 \times \text{TiO}_2 \text{ (spinel)}^{0.6322}$$

Augé (1987) has shown that the FeO/MgO ratio in chromian spinels is strictly dependent on the FeO/MgO ratio in the parental melt and he proposed an empirical formula for calculating the FeO/MgO ratio in the parental melt as follows:

$$\text{Ln}(\text{FeO/MgO})_{\text{(spinel)}} = 0.47 - 1.07Y^{\text{Al}}_{\text{(spinel)}} + 0.64Y^{\text{Fe}^{3+}}_{\text{(spinel)}} + \text{Ln}(\text{FeO/MgO})_{\text{(melt)}}$$

$$\text{Where: } Y^{\text{Al}}_{\text{(spinel)}} = \text{Al}/(\text{Al} + \text{Cr} + \text{Fe}^{3+}) \text{ and } Y^{\text{Fe}^{3+}}_{\text{(spinel)}} = \text{Fe}^{3+}/(\text{Al} + \text{Cr} + \text{Fe}^{3+}).$$

However, in order to test the validity of the application of the formulae proposed by these authors to the Mirdita ophiolites, a test using chromian spinels from volcanic rocks has been made. In this test we used chromian spinels compositions from three MTBs and two boninitic basalts from the Albanide-Hellenide ophiolites (Photiades et al., 2003; Sac-

cani and Photiades, 2005) assuming that whole-rock compositions represent liquid compositions. The Rollinson (2008) formulae proposed for MORB-type settings have been used for MTBs, whereas those proposed for arc-type settings have been used for boninitic basalts. In Fig. 8a the Al_2O_3 contents calculated from chromian spinels according to the formulae above are plotted against the Al_2O_3 content of their parental rocks. Both the methods proposed by Maurel and Maurel (1982) and Rollinson (2008) give calculated Al_2O_3 contents very similar to those of the parental rocks. Likewise, the TiO_2 contents calculated from chromian spinels plotted vs. the TiO_2 content of their parental rocks (Fig. 8b) show that the calculated TiO_2 contents are very similar to those really observed in the parental basalts. FeO/MgO ratios calculated using the Augé (1987) formula do not fully correspond to whole-rock FeO/MgO ratios (Fig. 8c). However, an acceptable correlation exists between calculated and observed FeO/MgO ratios (correlation coefficient $r^2 = 0.688$). It should be noted that, in contrast to Cr, Al, and Ti contents, subsolidus re-equilibration may change the FeO/MgO ratio in chromian spinels (Augé, 1987). This may explain the comparatively poorer correlation between calculated and observed FeO/MgO ratio. However, in Section 5.3 it has been shown that although these minerals experienced low-temperature re-equilibration, their composition was changed to a low extent during re-equilibration. Hence calculated FeO/MgO ratios can be reasonably used. Moreover, Fig. 8 shows that the formulae above give good results for a wide range of Al_2O_3 (10.06-17.67 wt%) and TiO_2 (0.16-0.91 wt%) contents and FeO/MgO ratios (0.59-0.83). Therefore, this test shows that the formulae above can be applied to the different varieties of ultramafic cumulates from the Mirdita ophiolites. The calculated Al_2O_3 , TiO_2 contents and FeO/MgO ratios of the parental melts with the Maurel and Maurel (1982), Rollinson (2008), and Augé (1987) formulae are shown in Table 2.

Ulmer (1989) demonstrated that the partition coefficient for Fe and Mg between olivine and melt is a function of melt composition and pressure and is essentially independent of temperature. From this relationship, it is possible to estimate the Mg# of a melt from which olivine has crystallized by using the plot in Fig. 8 of Ulmer (1989). Unfortunately, the pressure of crystallization of olivines in the

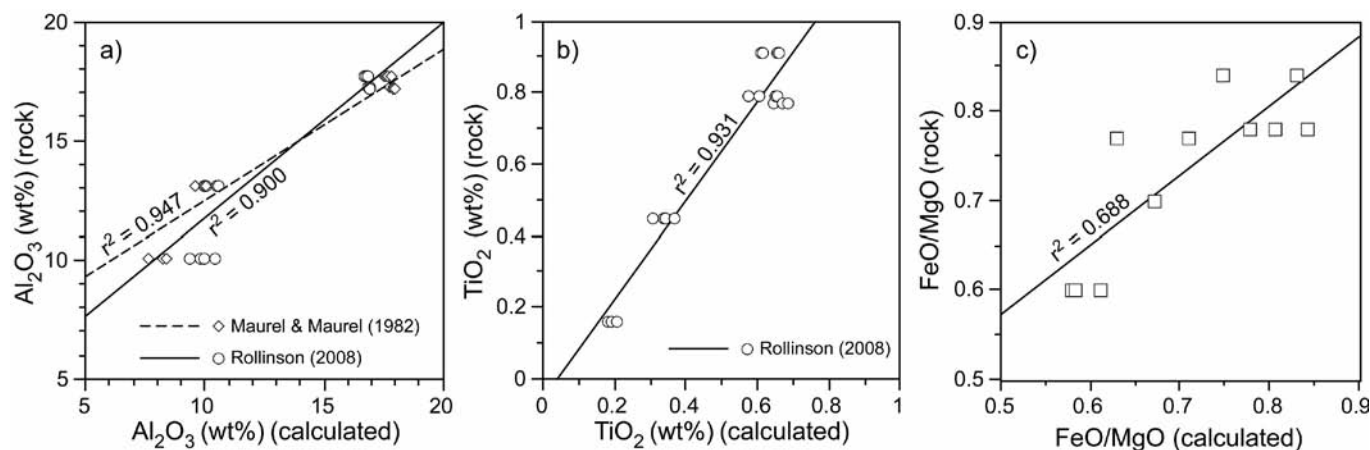


Fig. 8 - Correlation plots for Al_2O_3 (a), TiO_2 (b), and FeO/MgO ratios (c) in parental melts calculated from compositions of chromian spinel in representative boninitic and medium-Ti basalts from the Albanide-Hellenide ophiolites and the same oxides and oxides ratios observed in bulk rock. Mineral chemistry data from O. Zeda and E. Saccani (unpublished data), Bulk rock data from Photiades et al. (2003) and Saccani and Photiades (2005).

investigated rocks is unknown. Nonetheless, a valid estimation of the $Mg\#$ of parental melts can be made assuming a reasonable pressure range from 0.5 to 1 GPa. The mean $Mg\#$ of the olivine parental melts for each rock-type is shown in Table 1.

Western-type ophiolites

The calculated Al_2O_3 contents in parental melts for dunites and troctolites from the WMO is in the range ~14–18 wt%, which is the typical range of variation for MORB-type rocks (Fig. 9). However, the dunite AL9-troctolite AL10 pair shows TiO_2 contents ($TiO_2 = 0.80$ – 1.80 wt%) comparable to those of MORB-type rocks, whereas the dunite AL7-troctolite AL6 pair shows comparatively lower calculated TiO_2 contents (0.53–0.85 wt%), which are similar to those observed in MTBs and IATs from the Albanide-Hellenide ophiolites (Fig. 9). The calculated FeO/MgO ratios in parental melts display a wide range of variation (Fig. 10). Nonetheless, FeO/MgO ratios are comparatively lower in dunites (0.95–1.71) than in troctolites (1.26–2.62), which likely indicates derivation of dunites from primitive magmas and derivation of troctolites from slightly differentiated magmas. The co-variation of FeO/MgO ratios and Al_2O_3 contents (Fig. 10a) shows a coherent trend for all WMO cumulitic rocks. In contrast, the co-variation of FeO/MgO ratios and TiO_2 contents (Fig. 10b) shows two different trends for the AL7-AL6 and AL9-AL10 dunite-troctolite pairs. Using the plot in Fig. 8 of Ulmer (1989), we deduce that olivine from cumulitic dunites ($Mg\# = 0.88$ – 0.90) at pressures from 0.5 to 1.0 GPa equates to melts with $Mg\#$ ranging from 0.70 to 0.74. Olivines from troctolites ($Mg\# = 0.69$ – 0.73) are consistent with parental melts having $Mg\#$ in the range 0.69–0.71. These values are consistent with either MORB-type or MTB-type parentage.

Eastern-type ophiolites

The calculated Al_2O_3 (~7–14 wt%) and TiO_2 (0.10–0.24 wt%) contents in parental melts for chromitiferous-dunite, dunite, lherzolite, and Kukes olivine-websterite are very low and are comparable to those of boninitic rocks (Fig. 9). In contrast, plagioclase-dunite AL71 from the Krasta series and olivine-websterite from the Shebenik massif, though showing very low TiO_2 contents, display rather high Al_2O_3 contents (Fig. 9). TiO_2 content in parental melt for plagioclase-dunite AL70 (Krasta series) is comparatively higher (0.46–0.61 wt%) and is comparable to that of IATs or MTBs (Fig. 9). Plagioclase-dunite from the Krrab massif and plagioclase-lherzolites from both Kukes and Shebenik massifs have calculated Al_2O_3 (~14–16 wt%) and TiO_2 (1.19–1.76 wt%) contents, which are comparable to those typically observed in MORB-type rocks.

The co-variation of FeO/MgO ratios and Al_2O_3 contents (Fig. 10a) shows two different trends for the EMO cumulitic rocks. One trend of variation is represented by dunites and chromitiferous-dunites, which show a trend compatible with generation from boninitic liquids. The other trend is represented by (in order of increasing FeO/MgO ratios) plagioclase-dunites, plagioclase-lherzolite, troctolite, and lherzolite. In contrast, the co-variation of FeO/MgO ratios and TiO_2 contents (Fig. 10b) shows a well-defined trend including chromitiferous-dunites, dunites, lherzolites, and olivine-websterites, which is compatible with boninitic parental melts. The other rocks do not show any clear trend of variation. Plagioclase-dunites from Krasta have FeO/MgO ratios and TiO_2 contents similar to those of IAT rocks, whereas

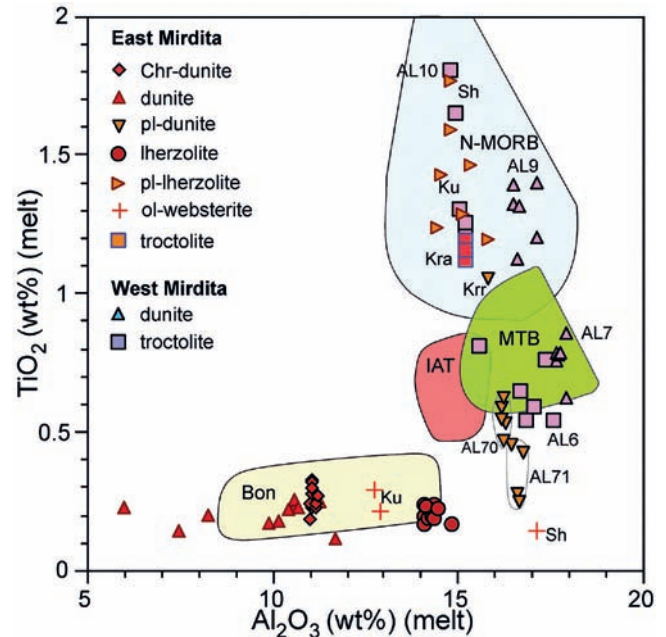


Fig. 9 - Plot of TiO_2 vs. Al_2O_3 contents in parental melts calculated from compositions of chromian spinel from ultramafic cumulates from the Mirdita ophiolites. The compositions of normal-type mid-ocean ridge (N-MORB), medium-Ti (MTB), island arc tholeiitic (IAT), and boninitic basalts from the Albanide-Hellenide ophiolites (Saccani and Photiades, 2005; Bortolotti et al., 2006; 2008; Dilek et al., 2008; Saccani et al., 2011) are reported for comparison. Abbreviations as in Fig. 3.

Krrab plagioclase-dunite, Kukes plagioclase-lherzolites, and Krasta troctolite have FeO/MgO ratios and TiO_2 contents similar to those of the AL9-AL10 dunite-troctolite pair from the WMO.

Tectono-magmatic implications

Four distinct types of basaltic rocks formed at both mid-ocean spreading ridge (i.e., N-MORB) and SSZ settings (i.e., MTB, IAT, and boninites) coexisted in both time and space in the Mirdita ophiolites during Jurassic time. In brief, N-MORB, MTB and boninitic basalts can be observed in the WMO, whereas IAT and boninitic basalts largely prevail in the EMO, together with very subordinate MORB magmatism (e.g., Beccaluva et al., Shallo, 1994; 1994; Bortolotti et al., 1996; Bébien et al., 2000; 2002; Robertson and Shallo, 2000; Hoeck et al., 2002; Saccani et al., 2011). The geochemical characteristics of these different magma-types, the nature of their mantle sources, and their mechanisms of formation are summarized below using the composition of primary basaltic rocks found in various localities of the Mirdita ophiolites (for a detailed review, see Saccani et al., 2011).

N-MORBs are typified by relatively high TiO_2 (> 0.90 wt%) and Al_2O_3 (~13–18 wt%) content, as well as relatively high FeO/MgO ratios (0.77–2.0). They have abundant high field strength element (HFSE) concentrations ($HFSE/N-MORB = 1$ – 5) and significant light REE (LREE) depletion ($La_N/Sm_N = 0.36$ – 0.63 ; $La_N/Yb_N = 0.48$ – 0.72). In contrast, MTBs show TiO_2 and Al_2O_3 contents varying from 0.67 to 1.10 wt% and from 15.70 to 18.75 wt%, respectively. Primary MTBs show FeO/MgO ratios slightly lower (0.64–1.23), when compared to N-MORBs. MTBs typically have severe Th, Nb, and LREE depletion (e.g., $La_N/Sm_N = 0.15$ – 0.28).

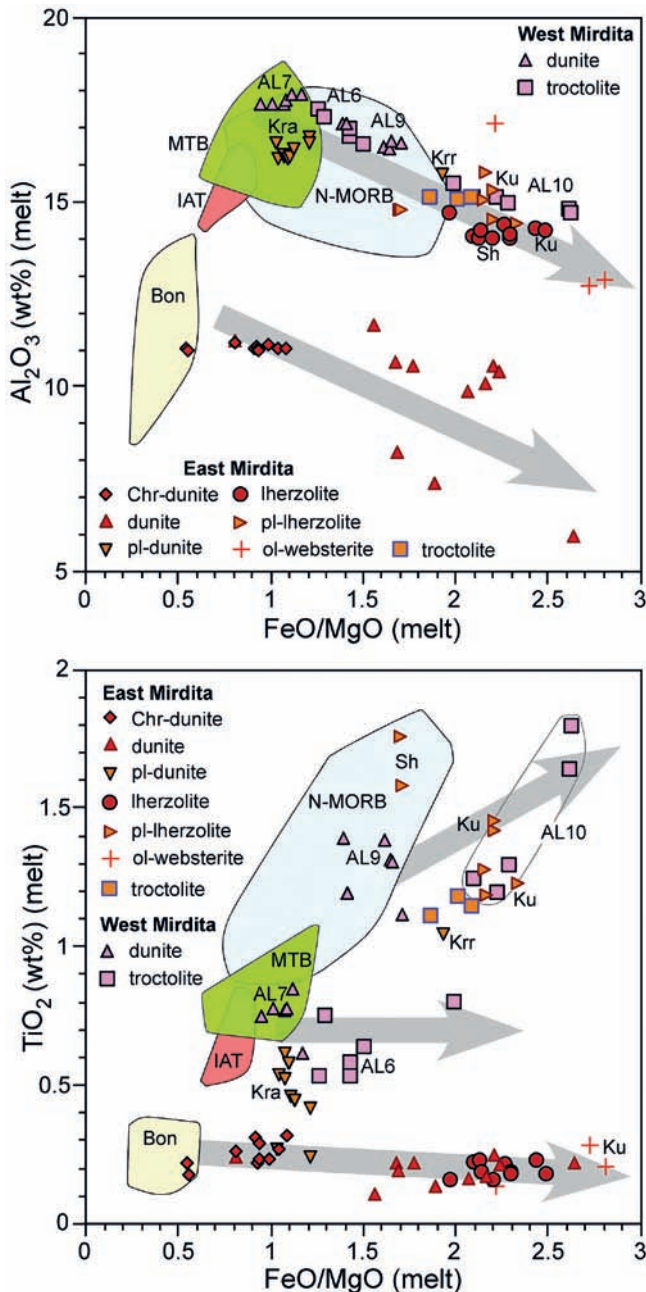


Fig. 10 - Plot of FeO/MgO ratios vs. Al_2O_3 contents (a) and TiO_2 contents (b) in parental melts calculated from compositions of chromian spinel in ultramafic cumulates from the Mirdita ophiolites. The composition of normal-type mid-ocean ridge (N-MORB), medium-Ti (MTB), island arc tholeiitic (IAT), and boninitic basalts from the Albanide-Hellenide ophiolites (Saccani and Photiades, 2005; Bortolotti et al., 2006; 2008; Dilek et al., 2008; Saccani et al., 2011) are reported for comparison. Arrows roughly indicate evolutionary trends. Abbreviations as in Fig. 3.

IAT basaltic rocks range in TiO_2 from 0.47 to 0.84 wt% and in Al_2O_3 from 13.95 to 18.75 wt%. They show relatively lower FeO/MgO ratios (0.65 - 0.83) compared to N-MORBs and MTBs. IATs are characterized by depletion in LREE, as exemplified by the La_N/Sm_N and La_N/Yb_N ratios ranging from 0.15 to 0.64 and 0.11-0.56, respectively. Boninitic basalts and basaltic andesites are typically characterized by very low TiO_2 contents (0.12-0.40 wt%), coupled with low Al_2O_3 contents (8.55-14.40 wt%) and high amounts of MgO (9.62-16.72 wt%), which result in very low FeO/MgO ratios

(0.25-0.57). They are also characterized by severe HFSE and REE depletions, as well as by both LREE depleted and U-shaped chondrite-normalized patterns.

N-MORBs primary magmas derived from ~10-20% partial melting of a primitive asthenospheric mantle. MTB and IAT primary magmas derived from ~10% and 10-20% partial melting of the MORB residual mantle, respectively. However, the most striking difference between MTBs and IATs is that the former have strong Th depletion, whereas the latter have relative Th enrichment. This implies that, while IAT magmas experienced SSZ-type enrichment by fluids released from the subducting slab, MTB melts were formed by partial melting of depleted peridotites, which did not experienced the addition of subduction components. Based on these features, Saccani et al. (2011) suggested that MTB were originated at a nascent forearc setting, whereas IAT were originated in an intra-oceanic arc. Boninitic primary magmas may have originated either from 10-20% partial melting of the MTB and IAT residual mantle or from ~30% partial melting of the MORB residual mantle. In both cases, the depleted mantle sources were enriched in LREE by subduction-derived fluids.

The calculated compositions of parental melts in equilibrium with olivine and spinels in the dunite-troctolite pair from the top of the ultramafic layered series of the Skanderbeu massif (WMO) suggest that these rocks likely derived from a MORB-type parental melt. The inferred liquid composition is indeed characterized by high TiO_2 , Al_2O_3 contents and FeO/MgO ratios (Figs. 9, 10). In contrast, the inferred liquid composition for the dunite-troctolite pair from the mantle tectonite-ultramafic cumulate transition zone from the Skanderbeu massif is characterized by high Al_2O_3 contents coupled with relatively low TiO_2 contents similar to those of MTBs (Fig. 9). Accordingly, the calculated FeO/MgO ratios in these rocks are slightly lower than those observed in the dunite-troctolite pair from the top of the ultramafic layered series and are generally compatible with MTB parentage (Fig. 10). Likewise, the Mg# in parental melt calculated from olivine composition in dunite AL7 is slightly higher than that calculated for dunite AL6 (Table 1) and, again, is consistent with MTB parentage. Therefore, we infer that the dunite-troctolite pair likely derived from MTB-type melts injected into the mantle tectonite-ultramafic cumulate transition zone of the Skanderbeu massif. This conclusion is in agreement with the crystallization order observed in MTB melts, which is: olivine \pm chromian spinel + plagioclase + clinopyroxene (Saccani et al., 2011) and can thus account for the formation of cumulitic dunites and troctolites during the early phases of fractional crystallization.

The calculated compositions of parental melts in equilibrium with olivine and spinels in chromitiferous dunites, dunites, lherzolites, and olivine websterites from the EMO suggest that these rocks likely derived from a boninitic-type parental melt. In fact, the inferred Al_2O_3 and TiO_2 contents are very low (Fig. 9). However, the FeO/MgO ratios calculated from spinel compositions show a wide range of variation (Fig. 10), which cannot be explained with primary boninitic melt parentage alone. Therefore, we infer that chromitiferous-dunites and dunites showing the lowest FeO/MgO ratios likely derived from relatively primitive boninitic melt. In contrast, lherzolites and olivine websterites having the highest FeO/MgO ratios may have derived from slightly fractionated boninitic melts. This conclusion is also supported by the Mg# in parental melts inferred from olivine compositions (Table 1).

The calculated compositions of spinel parental melts for plagioclase-dunite from the Krrab massif, plagioclase-lherzolites from the Kukes and Shebenik massifs, as well as for the Krasta troctolite show high TiO_2 and Al_2O_3 contents, as well as FeO/MgO ratios (Figs. 9, 10), which suggest a clear MORB-type parentage. In contrast, the affinity of the parental melt(s) for plagioclase-dunites from the Krasta series cannot straightforwardly be inferred. The calculated Al_2O_3 contents are rather high, suggesting a MORB-type or MTB-type parentage. Nonetheless, the calculated TiO_2 contents and FeO/MgO ratios range from low to very low (Figs. 9, 10) and are compatible with a SSZ-type melt parentage. Also the $\text{Mg}\#$ in parental melt inferred from olivine chemistry is rather high (Table 1) and resembles that of boninitic or IAT magma-types. Several hypotheses can be postulated for explaining this inferred parental melt chemistry. These rocks can be derived from slightly differentiated boninitic melts relatively enriched in Al_2O_3 . However, this hypothesis is in contrast with the inferred high $\text{Mg}\#$, which rather indicates a primitive liquid parentage. Alternatively, these rocks may have derived from MTB or IAT melts-types. A parentage with both these melt-types would be consistent with relatively high Al_2O_3 contents and low FeO/MgO ratios. Nonetheless, a genesis from IAT-type melts would better explain the low inferred TiO_2 contents.

Moreover, Al_2O_3 equilibrium in chromian spinels and parental melt can be modified by the presence of crystallizing plagioclase (Augé, 1987). Petrographic evidence indicates some amounts of trapped, intercumulus liquid crystallizing plagioclase. Therefore, we favour the hypothesis of low-Ti tholeiitic parentage and we postulate that the decoupling between the inferred high concentration of Al_2O_3 and low TiO_2 contents and FeO/MgO ratios in parental melt is likely due to reaction between plagioclase and spinel parental melt. From Figs. 9, 10 it is quite evident that no co-magmatic relationships between plagioclase lherzolites and troctolite from the Krasta series can be postulated. In fact, this hypothesis would imply a marked increase in TiO_2 contents and FeO/MgO ratios from plagioclase-lherzolites parental melt ($\text{TiO}_2 < 0.60$ wt%; $\text{FeO}/\text{MgO} = < 1.2$) to troctolite parental melt ($\text{TiO}_2 > 1.10$ wt%; $\text{FeO}/\text{MgO} > 1.9$). Nonetheless, mass balance shows that such a marked TiO_2 and FeO/MgO increase would imply a parental low-Ti liquid evolution from basaltic to andesitic composition, which is not compatible with petrographic observations.

In summary, from the discussion above it results that the cumulitic sequence in the WMO, though largely consisting of rocks showing N-MORB type parentage, also includes rocks formed from MTB-type parental melts originating, in turn, in a nascent forearc setting. Both MORB-type and MTB-type cumulates have their chemical equivalents in the WMO volcanic sequence. Likewise, the parental melts of ultramafic cumulates from the EMO show large variation including mainly boninitic and MORB compositions, as well as minor to IAT compositions. Chromiferous-dunites, dunites, lherzolites, and olivine-websterites were originated from boninitic parental melts. In contrast, plagioclase-bearing dunites and lherzolites, as well as troctolites were originated from MORB-type melts. Only one plagioclase-lherzolite from the Krasta series, though with some uncertainty, can be associated with IAT melt. Boninitic and IAT melts also resulted in large volumes of volcanic rocks in the EMO, whereas MORBs are not represented in this unit, with the exception of one basaltic dyke showing isotopic compo-

sition typical of the WMO rocks (Dilek et al., 2008). In any case, results on ultramafic cumulates further support the evidence that Mirdita ophiolites experienced the contemporaneous existence of different magma-types generated from distinct mantle sources.

Geodynamic models

Several models have been provided to explain the contemporaneous formation of MORB-type and SSZ-type melts, as well as their mutual relationships in the Mirdita ophiolites (Bébién et al., 2000; Insergueix-Filippi et al., 2000; Bortolotti et al., 2002; Hoeck et al., 2002; Dilek et al., 2008; Saccani et al., 2011). Insergueix-Filippi et al. (2000) have shown that the formation of MTBs from partial melting of a depleted mantle without a significant contribution from SSZ fluids requires an anomalously high thermal regime. Therefore, though with some variants, Bébién et al. (2000), Bortolotti et al. (2002) and Hoeck et al. (2002) suggested that subduction was established close to an active mid-ocean ridge. In this model, MTBs were generated from partial melting of relatively hot, depleted peridotites in a nascent forearc setting that was thermally perturbed by the nearby active mid-ocean ridge, which contemporaneously produced MORB-type melts. Meanwhile, the proto-forearc evolved to an intra-oceanic arc setting where IAT and boninitic melts were generated from partial melting of hydrous and progressively depleted, refractory peridotite in a rapidly evolving supra-subduction mantle wedge. According to this model, the WMO was located close to, or partially above the SSZ, so that boninitic melts were intruded as dykes and emplaced as lava flows into the MORB-MTB sequence of the WMO. Likewise, the proximity of MORB-type and SSZ-type sources allowed minor, late MORB-type melts to be produced almost contemporaneously to boninitic melts and to be injected into the EMO SSZ-type ophiolites. This model implies a general magmatic evolution from MORB to MTB, boninite and IAT melts.

An alternative model was proposed by Dilek et al. (2008). In this model, the WMO and EMO record a progressive evolution from MORB to IAT and boninitic magmas within the same SSZ tectonic environment (namely, an arc-protarc setting), which experienced rapid slab retreat during and after its initiation. During the evolution of the WMO and EMO, generation of different melts, aggregation/mixing, and differentiation probably occurred in multiple levels in the sub-arc and forearc mantle. According to this model, the MORB to SSZ transition is recorded from west (WMO) to east (EMO) and stratigraphically upward within each ophiolitic unit. The chemical progression towards the east resulted from an eastward shift in protoarc-forearc magmatism in consequence of slab rollback in this direction. Mantle flow above the retreating slab and in the arc-wedge corner played a major role in the formation and evolution of the different magma-types. MORB-type melts and, possibly, MTB-type melts (not considered in this model) were produced in the WMO from mantle sources with no detectable subduction influence. In contrast, progressive, consistent enrichment of SSZ components led to the formation of boninitic and IAT melts in the EMO.

Another model that can explain the magmatic evolution of MORB-type and SSZ-type melts in the Mirdita ophiolites is the "subduction initiation rule" proposed by Whattam and

Stern (2011). This model is based, in turn, on the “subduction infancy” model of Stern and Bloomer (1992), which was developed based on the magmatic evolution observed in the modern Izu-Bonin-Mariana (IBM) forearc. According to this model (see Fig. 2 in Whattam and Stern, 2011), the very early stages of subduction initiation involve decompression melting of a fertile, lherzolitic, asthenospheric source to form early MORB-type suites. MORB-type magmas were not formed at mid-ocean ridges, but are indistinguishable from those generated by seafloor spreading at true mid-ocean ridges. The contribution of fluids from dehydrating oceanic crust and sediments on the sinking slab is negligible in early subduction initiation, but continued melting results in a depleted, harzburgitic residue that was progressively metasomatized by fluids from the sinking slab. Subsequent partial melting of this source had then produced SSZ-type magmas (i.e., IAT and boninites) and possibly boninitic lavas and dykes at the latest stage.

All the models described above can broadly account for the coexistence in both time and space of MORB-type and SSZ-type magmas in the Mirdita ophiolites. A detailed discussion of these models in order to understand which one of them would be more appropriate for explaining the tectono-magmatic evolution of the Mirdita ophiolites is beyond the scope of this paper. In fact, such a discussion would require an exhaustive analysis of a number of geological, tectonic, stratigraphic features, including a discussion about the existence of a single oceanic basin or two separate oceanic branches in the Albanide-Hellenide Neo-Tethys. Nonetheless, some general remarks are worth to be made. The Dilek et al (2008) model perfectly account for the magmatic evolution and formation of the Mirdita ophiolites only assuming that these ophiolites were formed in a small, short lived marginal basin (i.e., the Jurassic Mirdita-Pindos basin) separated from the main Vardar ocean, as indeed coherently assumed by these authors. In contrast, assuming that the Mirdita-Pindos Ocean represented a wide, long lasting (i.e., Mid-Triassic-Late Jurassic) oceanic domain or that the Mirdita ophiolites were generated within a single Neo-Tethyan ocean (i.e., the Vardar Ocean), this model would not fully explain the magmatic events occurred from Mid-Triassic to Mid Jurassic.

The “subduction initiation rule” (Whattam and Stern, 2011) implies a diagnostic magmatic chemostratigraphic progression from less to more HFSE-depleted and large ion lithophile element (LILE)-enriched compositions, as in fact observed in the IBM system. Specifically, from MORB-type to arc-type magmas; that is, from subduction initiation to the establishment of a mature subduction zone. This chemostratigraphic progression is generally observed in the WMO and in its southward equivalent in the Pindos Massif. However, considering the WMO and EMO as a whole, the observed magmatic evolution is from LILE-depleted MORB-type to extremely LILE-depleted MTB-type magmas, then to LILE-enriched boninites and IAT associated again with LILE-depleted MORB-type melts. Hence, the Whattam and Stern (2011) model can hardly explain the occurrence of MORB-type melts associated with IAT and boninitic melts generated during the mature subduction zone stage. In summary, we favour the hypothesis that the Mirdita ophiolites formed in a nascent forearc setting established close to an active mid-ocean ridge that subsequently evolved to a mature intra-oceanic arc (Insergueix-Filippi et al., 2000; Bébien et al., 2000; Bortolotti et al., 2002; Hoeck et al., 2002). In particular, results of the nu-

merical modelling shown in Figs. 2, 3 of Insergueix-Filippi et al. (2000) can account for the relatively late formation of MORB-type melts during the mature subduction zone stage in consequence of the upwelling of MORB-type asthenosphere triggered by mantle flow above the subduction slab.

CONCLUSION

Chromian spinels and olivines occur in mantle peridotites and overlying ultramafic cumulates in both the WMO and EMO. Hence, we used the chemical compositions of these minerals for constraining the compositions of the parental melts from which they crystallized. The results can be summarized as follows.

1) Olivines and spinels from WMO mantle lherzolites indicate that these rocks represent abyssal-type peridotites, which experienced < 10% MORB-type melt extraction.

2) Olivines and spinels from ultramafic cumulates of the Skanderbeu massif in the WMO suggest that the stratigraphically lower ultramafic cumulates were derived from a N-MORB type parental melt. In contrast, the stratigraphically upper cumulitic series was derived from a MTB-type parental melt originated, in turn, in a nascent forearc setting.

3) Olivines and spinels from EMO mantle harzburgites indicate that these rocks represent SSZ-type residual peridotites, which experienced from 20 to 30% melt extraction.

4) Spinels in chromitiferous dunites, dunites, lherzolites, and olivine-websterites from the EMO show very low TiO₂ contents and generally high Cr#. The inferred compositions of parental melts suggest a boninitic parentage for these rocks.

5) Spinels in plagioclase-dunites, plagioclase-lherzolites, and troctolites from the EMO have relatively high Al₂O₃ and MgO contents and low Cr₂O₃ concentrations, whereas TiO₂ in these minerals show a wide range of variation. The inferred parental melt compositions are compatible with an N-MORB type parentage, being the only exception one plagioclase-dunite, which may have derived from a low-Ti tholeiitic melt.

6) Comparison of the ultramafic cumulates from the WMO and EMO indicates that both these units, though to different extents, have experienced similar and coeval magmatic events. The investigated WMO ultramafic cumulates record N-MORB and MTB magmatic episodes. The investigated EMO ultramafic cumulates testify for boninitic, N-MORB, and very subordinate low-Ti tholeiitic magmatic events. It is therefore concluded that both WMO and EMO were generated in a protoforearc - forearc setting likely initiated nearby an active mid-ocean spreading ridge.

ACKNOWLEDGMENTS

Special thanks go to Ottavia Zeda (Dipartimento di Fisica e Scienze della Terra, Università di Parma, Italy), who carried out most of mineral phase analyses. Many thanks go to R. Carampin and A. Fioretti (IGG-CNR, Padua) for their support with the EPMA analyses, as well as to M. Bonora for thin-section preparation. L. Beccaluva (Ferrara University), and I. Prempti (GjeoAlba, Tirana, Albania) are acknowledged for their help during field work. We would also like to thank M.C. Göncüoğlu and A. Montanini for their constructive review of this paper.

REFERENCES

- Ahmed A.H., Arai S. and Attia A.K., 2001. Petrological characteristics of podiform chromitites and associated peridotites of Pan African Proterozoic ophiolite complex of Egypt. *Mineral. Dep.*, 36: 72-84.
- Arai S., 1994. Characterization of spinel peridotites by olivine-spinel compositional relationships: Review and interpretation. *Chem. Geol.*, 113: 191-204.
- Augé T., 1987. Chromite deposits in the northern Oman ophiolite: mineralogical constraints. *Mineral. Dep.*, 22: 1-10.
- Ballhaus C., Berry R.F. and Green D.H., 1991. High pressure experimental calibration of the olivine-orthopyroxene-spinel oxygen geobarometer: implications for the oxidation state of the upper mantle. *Contrib. Mineral. Petrol.*, 107: 27-40.
- Barnes S.J. and Roeder P.L., 2001. The range of spinel composition in terrestrial mafic and ultramafic rocks. *J. Petrol.*, 42: 2279-2302.
- Bébién J., Shallo M., Manika K. and Gega D., 1998. The Shebenik Massif (Albania): A link between MOR- and SSZ-type ophiolites? *Ophioliti*, 23: 7-15.
- Bébién J., Dimo-Lahitte A., Vergély P., Insergueix-Filippi D. and Dupeyrat L., 2000. Albanian ophiolites. I - Magmatic and metamorphic processes associated with the initiation of a subduction. *Ophioliti*, 25: 39-45.
- Beccaluva L., DiGirolamo P., Macciotta G., Morra V., 1983. Magma affinities and fractionation trends in ophiolites. *Ophioliti*, 8: 307-324.
- Beccaluva L., Coltorti M., Premti I., Saccani E., Siena F. and Zeda O., 1994. Mid-ocean ridge and suprasubduction affinities in the ophiolitic belts from Albania. *Ophioliti*, 19: 77-96.
- Bortolotti V., Kodra A., Marroni M., Mustafa F., Pandolfi L., Principi G. and Saccani E., 1996. Geology and petrology of ophiolite sequences in the Mirdita region (Northern Albania). *Ophioliti*, 21: 3-20.
- Bortolotti V., Marroni M., Pandolfi L., Principi G. and Saccani E., 2002. Interaction between mid-ocean ridge and subduction magmatism in Albanian ophiolites. *J. Geol.*, 110: 561-576.
- Bortolotti V., Chiari M., Fazzuoli M., Marcucci M., Photiades A. and Principi G., 2002. New geological observation and biostratigraphic data on the Argolis Peninsula: palaeogeographic and geodynamic implications. *Ophioliti*, 27: 43-46.
- Bortolotti V., Chiari M., Kodra A., Marcucci M., Mustafa F., Principi G. and Saccani E., 2004. New evidence for Triassic MORB magmatism in the northern Mirdita Zone ophiolites (Albania). *Ophioliti*, 29: 243-246.
- Bortolotti V., Chiari M., Kodra A., Marcucci M., Marroni M., Mustafa F., Prela M., Pandolfi L., Principi G. and Saccani E., 2006. Triassic MORB magmatism in the southern Mirdita zone (Albania). *Ophioliti*, 31: 1-9.
- Bortolotti V., Chiari M., Marcucci M., Photiades A., Principi G. and Saccani E., 2008. New geochemical and age data on the ophiolites from the Othrys area (Greece): Implication for the Triassic evolution of the Vardar Ocean. *Ophioliti*, 33: 135-151.
- Bortolotti V., Chiari M., Marroni M., Pandolfi L., Principi G. and Saccani E., 2013. Geodynamic evolution of the ophiolites from Albania and Greece (Dinaric-Hellenic belt): One, two or more oceanic basins? *Intern. J. Earth Sci.*, 102: 783-811, doi: 10.1007/s00531-012-0835-7.
- Capedri S., Venturelli G. and Toscani L., 1982. Petrology of an ophiolitic cumulate sequence from Pindos, Greece. *Geol. J.*, 17: 223-242.
- Chiari M., Marcucci M. and Prela M., 2002. New species of Jurassic radiolarian in the sedimentary cover of ophiolites in the Mirdita area, Albania. *Micropal.*, 48: 61-87.
- Dick H.J.B. and Bullen T., 1984. Chromian spinel as a petrogenetic indicator in abyssal and alpine-type peridotites and spatially associated lavas. *Contrib. Mineral. Petrol.*, 86: 54-76.
- Dilek Y., Shallo M. and Furnes H., 2005. Rift-drift, seafloor spreading, and subduction tectonics of Albanian ophiolites. *Intern. Geol. Rev.*, 47: 147-176.
- Dilek Y., Furnes H. and Shallo M., 2008. Geochemistry of the Jurassic Mirdita Ophiolite (Albania) and the MORB to SSZ evolution of a marginal basin oceanic crust. *Lithos*, 100: 174-209.
- Droop G.T.R., 1987. A general equation for estimating Fe³⁺ concentrations in ferromagnesian silicates and oxides from microprobe analyses, using stoichiometric criteria. *Mineral. Mag.*, 51: 431-435.
- Fabriès J., 1979. Spinel-olivine geothermometry in peridotites from ultramafic complexes: *Contrib. Mineral. Petrol.*, 69: 329-336.
- Franz L. and Wirth R., 2000. Spinel inclusions in olivine of peridotite xenoliths from TUBAF seamount (Bismark Archipelago/Papua New Guinea): evidence for the thermal and tectonic evolution of the oceanic lithosphere. *Contrib. Mineral. Petrol.*, 140: 283-295.
- Hoeck V. and Koller F., 1999. The Albanian ophiolites and the Dinaride-Hellenide framework. *EUG-10, Strasbourg. J. Conference Abstr.*, 4: 406.
- Hoeck V., Koller F., Meisel T., Onuzi K. and Kneringer E., 2002. The Jurassic South Albanian ophiolites: MOR- vs. SSZ-type ophiolites. *Lithos*, 65: 143-164.
- Hoeck V., Ionescu C. and Onuzi K., 2014. The Southern Albanian ophiolites. *CBGA 2014 Field Trip FT5. Bul. Shkencave Gjeol.*, 7/2014, Spec. Iss.: 48 pp.
- Insergueix-Filippi D., Dupeyrat L., Dimo-Lahitte A., Vergely P. and Bébién J., 2000. Albanian ophiolites. II - Model of subduction zone infancy at a Mid-ocean ridge. *Ophioliti*, 25: 47-53.
- Jones G., Robertson A.H.F. and Cann J.R., 1991. Genesis and emplacement of the supra-subduction zone Pindos ophiolite, northwestern Greece. In: Tj. Peters, A. Nicolas and R.J. Coleman (Eds.), *Ophiolite genesis and evolution of the oceanic lithosphere*, Ministry Petrol. Minerals, Sultanate of Oman, Kluwer Acad., Norwell, p. 771-799.
- Kamenetsky V.S., Crawford A.J. and Meffre S., 2001. Factors controlling chemistry of magmatic spinel: an empirical study of associated olivine, Cr-spinel and melt inclusions from primitive rocks. *J. Petrol.*, 42: 655-671.
- Kepezhinskas P.K., Taylor R.N. and Tanaka H., 1993. Geochemistry of plutonic spinels from the north Kamchatka arc: comparisons with spinels from other tectonic settings. *Mineral. Mag.*, 57: 575-589.
- Koller F., Hoeck V., Meisel T., Ionescu C., Onuzi K. and Ghega D., 2006. Cumulates and gabbros in southern Albanian ophiolites: their bearing on regional tectonic setting. In: A.H.F. Robertson and D. Mountrakis (Eds.), *Tectonic development of the eastern mediterranean region*. *Geol. Soc. London Spec. Publ.*, 260: 267-299.
- Lee Y.I., 1999. Geotectonic significant of detrital chromian spinel: a review. *Geosci. J.*, 3: 23-29.
- Manika K., Shallo M., Bébién J. and Gega D., 1997. The plutonic sequence of Shebenik ophiolite complex, Albania: evidence for dual magmatism. *Ophioliti*, 22: 93-99.
- Marcucci M., Kodra A., Pirdeni A. and Gjata T., 1994. Radiolarian assemblages in the Triassic and Jurassic cherts of Albania. *Ophioliti*, 19: 105-114.
- Marcucci M. and Prela M., 1996. The Lumi i Zi, (Puke) section of the Kalor Cherts: Radiolarian assemblages and comparison with other sections in northern Albania. *Ophioliti*, 21: 71-76.
- Maurel C. and Maurel P., 1982. Étude expérimentale de la distribution de l'aluminium entre bain silicate basique et spinelle chromifère. Implications pétrogenétiques: teneur en chrome des spinelles. *Bull. Mineral.*, 105: 197-202.
- Murck B.W. and Campbell I.H., 1986. The effect of temperature, oxygen fugacity and melt composition on the behaviour of chromium in basic and ultrabasic melts. *Geochim. Cosmochim. Acta*, 50: 1871-1887.
- Parkinson I.J., Pearce J.A., 1998. Peridotites from the Izu-Bonin-Mariana forarc (ODP Leg 125): evidence for mantle melting and melt-mantle interaction in a suprasubduction zone setting. *J. Petrol.* 39: 1577-1618.

- Pearce J.A., Barker P.F., Edwards S.J., Parkinson I.J. and Leat P.T., 2000. Geochemistry and tectonic significance of peridotites from the South Sandwich arc-basin system, South Atlantic. *Contrib. Mineral. Petrol.*, 139: 36-53.
- Photiades A., Saccani E. and Tassinari R., 2003. Petrogenesis and tectonic setting of volcanic rocks from the Subpelagonian ophiolitic mélange in the Agoriani area (Othrys, Greece). *Ofioliti*, 28: 121-135.
- Pouchou J.L. and Pichoir F., 1985. PAP ϕ (pZ) procedure for improved quantitative microanalysis, In: J.T. Armstrong (Ed.), *Microbeam analysis*. San Francisco Press, San Francisco, p. 104-106.
- Robertson A.H.F., 1994. Role of the tectonic facies concept in orogenic analysis and its application to Tethys in the Eastern Mediterranean region. *Earth Sci. Rev.*, 37: 139-213.
- Robertson A.H.F. and Shallo M., 2000. Mesozoic-Tertiary tectonic evolution of Albania in its regional Eastern Mediterranean context. *Tectonophysics*, 316: 197-214.
- Roeder P.L., 1994. Chromite: from the fiery rain of chondrules to the Kilauea Iki lava lake. *Can. Mineral.*, 32: 729-746.
- Rollinson H., 2008. The geochemistry of mantle chromitites from the northern part of the Oman ophiolite: inferred parental melt compositions. *Contrib. Mineral. Petrol.*, 156: 273-288, doi: 10.1007/s00410-008-0284-2.
- Saccani E. and Photiades A., 2004. Mid-ocean ridge and supra-subduction affinities in the Pindos Massif ophiolites (Greece): Implications for magma genesis in a proto-forearc setting. *Lithos*, 73: 229-253.
- Saccani E. and Photiades A., 2005. Petrogenesis and tectono-magmatic significance of volcanic and subvolcanic rocks in the Albanide-Hellenide ophiolitic mélanges. *Isl. Arc*, 14: 494-516.
- Saccani E., Beccaluva L., Photiades A. and Zeda O., 2011. Petrogenesis and tectono-magmatic significance of basalts and mantle peridotites from the Albanian-Greek ophiolites and sub-ophiolitic mélanges. New constraints for the Triassic-Jurassic evolution of the Neo-Tethys in the Dinaride sector. *Lithos*, 124: 227-242, doi: 10.1016/j.lithos.2010.10.009.
- Saccani E., 2014. A new method of discriminating different types of post-Archean ophiolitic basalts and their tectonic significance using Th-Nb and Ce-Dy-Yb systematics. *Geosci. Front.*, <http://dx.doi.org/10.1016/j.gsf.2014.03.006>.
- Shallo M., 1994. Outline of the Albanian ophiolites. *Ofioliti*, 19: 57-75.
- Shallo M., Kodra A. and Gjata K., 1990. Geotectonics of the Albanian ophiolites. In: J. Malpas, E. Moores, A. Panayiotou and C. Xenophontos (Eds.), *Ophiolites: oceanic crustal analogues*. *Proceed. Symp. Troodos 1987*. *Geol. Surv. Cyprus, Nicosia*, p. 265-269.
- Stern R.J. and Bloomer S.H., 1992. Subduction zone infancy; examples from the Eocene Izu-Bonin-Mariana and Jurassic California arcs. *Geol. Soc. Am. Bull.*, 104: 1621-1636.
- Stevens R.E., 1944. Composition of some chromites of the western Hemisphere. *Am. Mineral.*, 29: 1-34.
- Ulmer P., 1989. The dependence of the Fe²⁺-Mg cation-partitioning between olivine and basaltic liquid on pressure, temperature and composition. *Contrib. Mineral. Petrol.*, 101: 261-273.
- Whattam S.A. and Stern R.J., 2011. The 'subduction initiation rule': a key for linking ophiolites, intra-oceanic forearcs, and subduction initiation. *Contrib. Mineral. Petrol.*, 162: 1031-1045, doi: 10.1007/s00410-011-0638-z.
- Xhomo A, Kodra A, Dimo L. et al., 2002. Geological Map of Albania 1: 200 000 scale. *Geol. Surv. Albania*.
- Zhou M.-F., Robinson P.T., Malpas J. and Li Z., 1996. Podiform chromitites in the Luobusa ophiolite (southern Tibet): implications for melt-rock interaction and chromite segregation in the upper mantle. *J. Petrol.*, 37: 3-21.

Received, February 5, 2015

Accepted, April 22, 2015